Plasma Transport from A Deformed Magnetotail to The High-latitude Atmosphere Manifested by A Nightside Distorted Auroral Transpolar Arc

Motoharu Nowada[1], Qiu-Gang Zong[2], Benoît Hubert[3], Quan-Qi Shi[1], Yong-Fu Wang[2], Jun Yang[1], Adrian Grocott[4], Alexander W. Degeling[1], An-Min Tian[1], Xu-Zhi Zhou[2], and Chao Yue[2]

[1]Shandong Provincial Key Laboratory of Optical Astronomy and Solar-Terrestrial Environment, Institute of Space Sciences, Shandong University, Weihai, People's Republic of China.

[2]Institute of Space Physics and Applied Technology, School of Earth and Space Sciences, Peking University, People's Republic of China.

[3]Space science, Technologies and Astrophysics Research (STAR) Institute, Université de Liège, Belgium.

[4] Space and Planetary Physics Group, Department of Physics, Lancaster University, Lancaster, UK.

Key points:

1. A new morphological type of transpolar arcs, characterized by large nightside distortions in the pre- or post-midnight sector, is described.
2. Nightside reconnection and magnetotail deformation by the IMF penetration play an essential role in the nightside distorted TPA formation.
3. The nightside distorted TPAs can be used as a remote-sensing tool to diagnose the globally IMF-deformed magnetospheric processes.

Corresponding Authors:
Motoharu Nowada (moto.nowada@sdu.edu.cn),
Qiu-Gang Zong (qgzong@pku.edu.cn),
Quan-Qi Shi (sqq@sdu.edu.cn)

Abstract

The terrestrial magnetosphere is perpetually exposed, and significantly deformed by the Interplanetary Magnetic Field (IMF) in the solar wind. This deformation is typically detected at discrete locations by space- and ground-based observations. Earth's aurora, on the other hand, is a globally distributed phenomenon that may be used to elucidate magnetospheric deformations caused by variations in IMF, as well as plasma transport from the deformed magnetotail to high-latitude atmosphere. Here we report the utilization of an auroral form known as the transpolar arc (TPA) to diagnose the plasma dynamics of the globally deformed magnetosphere. Two types of new morphological TPAs, which are designated as "J"- and "L"-shaped TPAs based on their shape, are identified and shown to have antisymmetric morphologies in the Northern and Southern hemispheres, depending on the IMF polarity. The electric currents flowing aligned to the magnetic field lines which connect between the magnetotail and the auroral zone play an essential role in the formations of the "J"- and "L"-shaped TPAs. They can be induced by the velocity difference between the fast plasma flows associated with nightside magnetic reconnection and slower background plasma flows in the magnetotail. The interpretation of their features in a global context facilitates the usage of TPAs as a diagnostic tool to effectively remote-sense the globally deformed magnetospheric processes in response to the IMF conditions. Our results in this study contribute to understanding the influence of the IMF and solar wind plasma on auroral processes at Jupiter, Saturn, and the other planets of solar system.

Keywords: Nightside Distorted Transpolar Arc; Solar Wind-Magnetotail-High-latitude Atmosphere Coupling; Magnetospheric Diagnosis; Magnetotail Magnetic Reconnection; Plasma Flow Shear; Field-Aligned Currents

Plain Language Summary

Aurora is one of the important phenomena in qualitatively and quantitatively considering the circulations of the plasma and its energy from external solar wind to auroral zone via internal magnetosphere. To understand a global picture of the plasma transport from the terrestrial magnetotail deformed by the solar wind magnetic field (IMF) to the auroral zone, the formation process of a new morphological transpolar arc (TPA) is investigated in this study. The source of these TPAs is the electric currents flowing along the magnetic field lines, induced by the plasma flow velocity difference between the fast plasma flows generated by magnetotail reconnection and slower background magnetospheric plasma flows. The conventional TPA has a straight bar shape, which connects between nightside and dayside auroral ovals. However, new morphological TPAs in which we discovered have significant "distortions" toward pre- and post-midnight at their nightside ends, which would be caused by the magnetic field line twisting and magnetotail deformations due to the IMF penetrations. Our results facilitate a paradigm shift in understanding the implications of TPA structure on global-scale dynamics in the deformed magnetosphere, and as such, the usage of the auroral TPA shape as a tool to diagnose the global scale magnetospheric effects.

Introduction

The terrestrial magnetosphere dynamically changes through interactions with the high-speed streams of energetic particles (solar wind) and Interplanetary Magnetic Field (IMF) originating from the Sun, effectively shielding life on Earth from harmful radiation effects associated with these particles (Black, 1967; Glassmeier et al. 2009, 2010; Shi et al. 2013). The geomagnetic field surrounding the Earth also plays a role in preventing atmospheric oxygen from escaping into space (Wei et al. 2014). Therefore, it is important to understand the morphological features, formation, and dynamics of our terrestrial magnetosphere. In particular, the plasma transport between the magnetotail deformed by the IMF conditions and high-latitude atmosphere is one of the crucial magnetospheric processes.

Significant global magnetospheric effects are produced not only by changes in the IMF north-south component (IMF-B_z) but also its dawn-dusk component (IMF-B_y). A series of observational studies (Kaymaz et al. 1995; Nishida et al. 1995, 1998; Pitkänen et al. 2013, 2015, 2017) have found that under dominant IMF-B_y conditions, the magnetotail (plasma sheet) become increasingly twisted with down-tail distance, caused by the IMF-B_y penetration into the magnetotail. Magnetotail deformation and IMF penetration to the magnetotail have been attributed to magnetic reconnection under dominant IMF-B_y conditions (Gosling et al. 1990; Cowley, 1981, 1994; Tenfjord et al. 2015, 2018), which causes asymmetries in the magnetosphere. Inside the deformed magnetosphere, magnetic reconnection can occur and release energized plasma (electrons) earthward and tailward. The “source” of the aurora is the earthward transported energetic plasma. When magnetic reconnection occurs, magnetic energy stored in the magnetotail converts to particle kinetic energy, producing accelerated plasma flows out of the reconnection region as earthward and distant-tailward high-speed exhaust jets. As a result, localized fast plasma flows associated with reconnection are embedded within lower velocity plasma flows of magnetospheric origin in the magnetotail. Flow shear between high and low velocity flows generates electric currents that flow parallel to magnetic field lines, known as Field-Aligned Currents (FACs) (Hasegawa and Sato, 1979; Birn and Hesse, 1991; Fairfield et al. 1999). Evidence of this process has been compiled by sparse, spatially discrete ground-based, and space-based magnetic field and particle observations. However, the aurorae seen in the Northern and Southern hemispheres can be used as a tool to globally diagnose these magnetospheric processes.

A specific auroral form observed under northward IMF-B_z conditions, the Transpolar arc (TPA), occurs at extremely high latitudes. This is identified as a “bar-shaped” emission within the polar cap region, extending from the poleward edge of the nightside auroral oval toward the dayside (Frank et al. 1982). Its formation mechanism and features have been discussed based on magnetospheric convection and their relationship with the IMF orientation (Fear and Milan, 2012a, 2012b). TPA locations depend on the extent of clockwise or counter-clockwise plasma sheet twisting (viewed from the magnetotail), which is controlled by the IMF-B_y polarity (i.e. either dawnward or duskward, for clockwise or counter-clockwise twisting) (Tsyganenko and Fairfield, 2004; Tsyganenko and Stinov, 2005; Tsyganenko et al. 2015; Cumnock et al. 2002).

The nightside magnetic reconnection model (Milan et al. 2005) is one of the most representative TPA formation models, and has been applied to explain the developments of many TPAs (Fear and Milan, 2012a, b; Kullen et al. 2005; Nowada et al. 2018). In this model, the TPA growth is attributed to continual formation of newly closed field lines by magnetotail reconnection, whose location retreats tailward. Several “non-straight” TPAs were also identified in previous statistical studies (21, 28), which contrast with the “bar”-shaped TPA (hereafter, referred to as a “regular TPA”) previously discussed (Fear and Milan, 2012a, b; Kullen et al. 2005; Nowada et al. 2018). However, neither the physical mechanism for these TPAs, nor their implications to the IMF-deformed magnetospheric dynamics have been discussed.

In this paper, we firstly identify a new morphological type of nightside distorted TPAs, which are distinct from the “regular” TPAs. Utilizing space-borne image and in-situ magnetotail observations, together with ground-based geomagnetic field and high-frequency (HF) radar observations, we obtain a global picture of the plasma transport from the deformed magnetotail to high-latitude atmosphere (auroral zone) by considering their implications in the nightside distorted TPA formation. In so doing, we demonstrate that the nightside distorted TPAs can be used as a remote-sensing diagnostic tool for global magnetospheric effects.

Instrumentation

New morphological TPAs discussed in this paper were identified using a large database spanning 5 years of auroral observations from 2000 to 2005 by the Wideband Imaging Camera (WIC), which is part of the Far Ultraviolet (FUV) instrument (Mende et al. 2000a, b, c) onboard the Imager for Magnetopause-to-Aurora Global Exploration (IMAGE) , launched in March, 2000. IMAGE FUV-WIC imaged the aurora in a broad emissive spectral range from 140 nm to 190 nm with high spatial resolution and 2 minutes' cadence. From this database, we chose the 9 nightside distorted TPAs based on visual inspections, which were clearly imaged in the plots of the IMAGE FUV-WIC data after the removal of the background optical noise by image processing (i.e., the dayside glow contamination and instrumental optical noise) as described as follows.

The IMAGE FUV-WIC data frequently includes optical contamination, such as sunlight (dayglow) and instrumental optical noise. These non-auroral signals were removed as much as possible from the original WIC images by fitting a two-dimensional Fourier series over the dayglow and a two-dimensional polynomial over the nightside background. The auroral region is excluded from the fit, and the overlapping parts of both functions are included so that a smooth merging can be made near the terminator. A smooth (averaged) analytical representation of the non-auroral background is then obtained, and can be used to infer the non-auroral contribution over the whole image, including the auroral region. Because the noise generated by the bright dayglow can hardly be represented by this method, the optical contaminations cannot completely be cleaned from the image. However, these imager data via the optical noise removal process provide us opportunity enough to identify several fine nightside distorted TPAs.

Results

Overview of Nightside Distorted TPA

"Regular" TPAs generally have a straight shape connecting the nightside and dayside auroral oval. In contrast, all TPAs discussed in this paper have a significant "distortion" at the nightside ends (hereafter, referred to as "nightside distorted TPA"). Figure 1 shows false color images of 8 representative nightside distorted TPAs, which were identified from IMAGE-FUV-WIC observations. The top (bottom) row of panels correspond to cases of IMF-$B_y < 0$ (IMF-$B_y > 0$), and the first three columns show Northern hemisphere (NH) observations, while the last column displays Southern hemisphere (SH) observations. In each panel, the top and bottom corresponds to noon (12 MLT) and midnight (24 MLT), and the right and left sides correspond to dawn (6 MLT) and dusk (18 MLT) meridians, respectively. The color scale is expressed in Analogic-Digital Units (ADU), which is proportional to the observed auroral brightness (Mende et al. 2000b). The upper panels (a) to (c) display the dawnside TPAs with the nightside ends distorted toward midnight or pre-midnight observed in the NH. Hereafter, we identify these as "J"-shaped TPAs based on their resemblance to the letter "J". In all observed TPAs, the "J"-shaped TPAs in the NH occur during a negative (dawnward) IMF-B_y interval. In bottom panels (e) to (g), the nightside distorted TPAs with the opposite chirality occurred on the duskside, in which the nightside ends get distorted toward midnight or post-midnight. We identify them as "L"-shaped TPAs based on their resemblance to "L". Panels (d) and (h) show observations in the SH during negative and positive IMF-B_y intervals, respectively. Interestingly, these two panels appear to show the opposite chirality to their NH counterparts under the same IMF conditions, with an "L"-shaped TPA (panel d), and a "J"-shaped TPA (panel h). The detailed growth of the representative four nightside distorted TPAs and corresponding solar wind conditions are shown in Supporting Information (Figure S1).

In-situ Duskside Magnetotail Observations during the Nightside Distorted TPA interval

All of the "J (L)"-shaped TPAs identified in our study, shown in Figure 1, originate in the nightside main auroral oval and protrude to the dayside, advocating that nightside magnetic reconnection plays a significant role in the formation of these TPAs (see the detailed in a series of figures shown in Figure S1). In-situ magnetotail observations were examined during the nightside distorted TPA intervals. Figure 2 shows a summary plot of the solar wind (observed by Advanced Composition Explorer: ACE), and the magnetotail (observed by Geotail) on March 12th, 2002, when the "L"-shaped TPA was detected by IMAGE FUV-WIC. The panels from top to bottom show: the IMF-B_y and -B_z components in GSM coordinates, the solar wind dynamic pressure, the Geotail measurements of the sun-earth (GSM-X), dawn-dusk (GSM-Y) and north-south (GSM-Z) magnetic field components in the duskside magnetotail, the associated magnetic field elevation angle, and three components of the ion flow velocity over the 1 hour 40 minutes time interval between 00:10 UT and 01:50 UT. During this interval, the "L"-shaped TPAs (LS) were observed from 00:31:34 UT to 00:58:12 UT and from 01:10:29 UT to 01:37:07 UT, as bracketed by two gold broken lines. The GSM locations of Geotail when the "L"-shaped TPAs were seen are shown in the bottom of the panels. The IMF-B_y and -B_z components were oriented roughly duskward (positive) and northward (positive) during two TPA intervals. Associated solar wind dynamic pressure showed no significant changes. The large abrupt decrease and increase in the Geotail-B_x component indicate multiple crossings of the magnetotail current sheet. The variations of associated B_y and B_z components were anti-correlated with that of the B_x component. Particular enhancements of the B_z component and elevation angle, seen in both LS intervals, suggest that the nightside magnetospheric configuration becomes more "dipole-like", resulting from the pile-up of the magnetic flux transported from distant magnetotail. Before the B_z enhancements, the V_x components showed earthward "bursty" enhancements, indicating the occurrence of magnetotail magnetic reconnection at the onset and the initial stage of the two "L"-shaped TPAs. These earthward flow burst profiles also suggest the tailward retreat of the reconnection locations; the V_x component in the first interval had already started to decrease at the onset of the "L"-shaped TPA, and the flow burst velocity during the second "L"-shaped TPA interval was lower than that in first TPA interval (if considering that there was little difference in the satellite positions between first and second TPA intervals).

The panels (b) and (c) show zoomed-in plots of the three plasma flow velocity components in GSM coordinates (upper two panels) and the ground magnetic field perturbations in the B_N (local magnetic north-south) and B_E (local magnetic east-west) components measured at two representative ground magnetic observatories close to the TPA (lower panel). The detailed information of the ground stations is listed in Table S2 in order of high geographic latitude. In the first plasma flow burst (panel b), the peak of the V_x component and those in the ΔB_N components are seen at the same time, suggesting that the fast flows associated with magnetotail reconnection might trigger electric currents, and cause the variations of geomagnetic field. During the second flow burst interval, the geomagnetic field peaks were not seen as shown in panel (c). Therefore, at this stage, it remains unclear whether or not electric currents which would disturb the geomagnetic field were induced by reconnection-associated fast plasma flows in this case. The summary and zoomed-in plasma velocity plots from Geotail observations of the opposite dawnside magnetotail are shown in Supporting Information (Figure S2).

The Electric Current Inferred from The Ground

When the "flow velocity difference (flow shear)" between reconnection-associated earthward fast flows and slow magnetotail background flows is present, electric currents flowing aligned to the geomagnetic field lines (Field-Aligned Currents: FACs) can be driven (Hasegawa and Sato, 1979; Birn and Hesse, 1991; Fairfield et al. 1999). These FACs are closely related to auroral phenomena in high-latitude atmosphere. In order to investigate this current system, an electric current map is made based on the geomagnetic field variations measured at the ground observatories in the SuperMAG ground observatory network (Gjerloev, 2012) beneath and in close proximity to the regions of growth of the "L"-shaped TPAs. Figure 3 shows the current maps projected onto geomagnetic coordinates before and during the "L"-shaped TPAs, including the intervals of earthward flow bursts. The electric current maps near the "L"-shaped TPAs are derived based on perturbations of the local magnetic north – south (B_N) and east – west (B_E) components of the geomagnetic field which were measured at the ground magnetic observatories beneath and in close proximity to the growth regions of the nightside distorted TPA. It is well-known that these ground magnetic disturbances are generated by the horizontal components of electric currents in the auroral zone (Glassmeier et al. 1989). The geomagnetic field perturbations can be taken from 20-minute-high-pass filtered B_N and B_E components. Further electric current vectors are obtained by rotating these geomagnetic field fluctuation components 90 degrees clockwise. On the maps during both the first (a) and second (b) flow burst intervals, counter-clockwise current vortices were found as highlighted with cyan arrows and magenta circle arrows, explicitly suggesting that FACs generated by the plasma flow shear were launched from the auroral zone toward the magnetotail. This result is also clear evidence that the energized plasma (electrons) were transported by the magnetotail fast flows from the magnetotail to the auroral zone. Furthermore, the vortex spatial scale is different between first and second interval. In panel (a), a "large-scale" vortex-like current structure is discerned by the electric current vectors measured at most observatories, while "small-scale" current vortices with a similar rotational sense are indicated during the second interval (panel b). Neither vortex current structure showed any poleward (high-latitude) migration as the "L"-shaped TPA grew to the dayside.

Retreat of Reconnection Points

The electric current vortices suggest that FACs might be an essential mechanism to form the nightside distorted TPA. Here, we consider the "growth" of the TPA. According to conventional nightside reconnection model (Milan et al. 2005), which does not take into account the influence of FACs in the TPA formation, the reconnection points should retreat tailward as the TPA grows to the dayside. A summary plot in Figure 2 has already suggested the tailward retreat of the reconnection point. To further support the scenario, we examine the geomagnetic field variations associated with the nightside distorted TPAs using ground-based observations. Figure 4 shows a scatter plot of the fluctuation peaks in the local magnetic north-south magnetic field component (ΔB_N) at several ground magnetic observatories from geographical low- to high-latitudes against the time delay between the peak times and the onset times of the 5 nightside distorted TPAs. The locations of the observatories correspond to points beneath or in close proximity to the regions of growth of the nightside distorted TPAs. All magnetic field data for the ground observatories were taken from the SuperMAG network (Gjerloev, 2012). Detailed geomagnetic field plots and information on the ground magnetic observatories are shown in Supporting Information (Figure S3). All peaks seen in the magnetic field fluctuation components were positive, implying enhancements of FACs flowing out of the auroral zone, that is, downflowing of electrons from the magnetotail. In the three TPAs (2000/09/22, 2001/12/31 and 2002/03/02), the magnetic peaks are seen at later times for observatories with higher latitude, suggesting that the reconnection points (the source regions of the energetic electrons) were retreating further down-magnetotail, associated with the growth of the TPA to the dayside. This result supports not only the tail reconnection occurrence but also the retreat of the reconnection points. The average velocity of the reconnection point retreat can roughly be estimated based on the time delay between the magnetic peaks and the TPA onsets using a value of 1 degree = 110.95 km in geographic latitude. The estimated reconnection point retreat velocity is summarized in the table in the upper right of the figure. The three TPAs had the reconnection point retreat velocity within a range between about 1.2 km/s and 3.0 km/s, but the others (2000/11/05 and 2002/03/12) showed a much faster retreat speed (7.3 km/s and 12.3 km/s) because their magnetic field peaks appeared with much less time lags, irrespective of the latitudes of the observatory locations.

Persistence of Magnetotail Reconnection During the Northward IMF Interval

We discuss the plasma flows and their patterns in the polar cap region measured by Super Dual Auroral Radar Network High Frequency (SuperDARN HF) radars (Greenwald et al. 1995; Chisham et al. 2007) during the nightside distorted TPA intervals, in order to obtain evidence for the persistence of magnetotail magnetic reconnection even under the northward IMF conditions. The SuperDARN radar arrays, which are located in the high-latitude regions in both northern and southern hemispheres, provide line-of-sight plasma flow velocity. These measurements, particularly obtained from nine SuperDARN radars in the northern hemisphere, have been used to produce high-latitude convection maps based on the "Map Potential" technique (Ruohoniemi and Baker, 1998). The line-of-sight velocity vectors are projected onto geomagnetic grids, and fitted to electrostatic potential solutions, which are described by a sixth order spherical harmonic expansion. Complementary flow data from a statistical model characterised by upstream IMF conditions (Ruohoniemi and Greenwald, 1996) is used to constrain the construction of the large-scale flow pattern in regions where the radars provide no measurements (Ruohoniemi and Baker, 1998).

Figure 5 presents the 6 selected northern hemispheric plasma flow streamlines and drift velocity vectors during the interval of the nightside distorted TPA ("J"-shaped TPA) observed on 31st December 2001. We overlay these flow velocity profiles onto the corresponding IMAGE FUV-WIC auroral imager data. Black regions indicate higher auroral luminosity, and the IMAGE observational time is shown on the top in each panel. The left, bottom and right sides in each panel correspond to 18h, 24h, and 6h in magnetic local time, respectively. The dotted semicircles indicate the magnetic latitude (MLat) range between 60 degrees and 80 degrees. During the growth of the "J"-shaped TPA, westward plasma flows, ranging between 0.3 km/s and 0.55 km/s, were locally (although non-continuously) observed equatorward of the poleward edge of the midnight-sector main auroral oval, highlighted by magenta ovals. These flows were originally oriented toward the equator, but rotated toward the west at the poleward edge of the main auroral oval. They are highly suggestive of magnetic reconnection in the magnetotail, identified as "Tail Reconnection during IMF Northward and Non-substorm Intervals (TRINNIs)" (Grocott et al. 2003, 2004) under dawnward IMF-B_y conditions (see the IMF condition shown in Figure S1c) (Milan et al. 2005; Grocott et al. 2003, 2004). Therefore, at least, nightside reconnection was ongoing during the growth of the "J"-shaped TPA even under the northward IMF conditions, and should play a significant role in the nightside distorted TPA formation.

A Possible Formation Scenario of the Nightside Distorted TPA

The conventional nightside reconnection model (Milan et al. 2005) explains the TPA formation based on the magnetospheric convection of the magnetic fluxes formed by magnetotail reconnection. However, in our case, the FACs appear to play an essential role in the nightside distorted TPA formation. The ground-based observations revealed that the reconnection points retreated tailward with the poleward growth of the TPAs. Furthermore, the SuperDARN HF radar detected TRINNIs, which are remote-sensing evidence for persistent magnetotail reconnection even under the northward IMF conditions.

Taking into account these observations, we construct a model to illustrate the nightside distorted TPA ("L"-shaped TPA) formation. Figure 6 displays a schematic diagram of the possible formation process of an "L"-shaped TPA under positive IMF-B_y conditions. The main "bar-like" emissions of the nightside distorted TPAs are located on the dusk side under positive IMF-B_y conditions as seen in Figure 1. The location of the "L"- ("J")-shaped TPAs strongly depends on the IMF-B_y sign; the relation between the location of the main TPA part and the IMF-B_y polarity is the same as that for the "regular" TPA (Comnock et al. 2002; Kullen et al. 2002) (see the plots of the OMNI and Geotail-measured solar wind data in Figure S1). This model is depicted in terms of the configuration changes of magnetic field lines due to magnetospheric convection, FACs, reconnection-associated plasma flows, and the reconnection point retreat. The closed field lines formed by nightside reconnection are illustrated by thick blue solid curves, and the orange curves indicate the electric currents induced by the plasma flow shear between the background slow plasma flows and fast flows originating from magnetic reconnection (blue arrows). FACs flowing out of the auroral zone toward the magnetotail should be the "source" of the nightside distorted TPAs, being consistent with large- and small-scale electric current vortices beneath and in close proximity to the growth regions of the nightside distorted TPAs. Magnetotail reconnection continues at the point denoted by red dots until the TPA completely forms, and associated closed field lines convect earthward. The reconnection location retreats further tailward from T_0 to T_3, which are highlighted by the thick red arrows and pink-shaded area, as TPA approaches the dayside. This is because higher latitude field lines within the TPA have their nightside (equatorial crossing) positions further down-tail.

In the nightside distorted TPA, the reconnection points retreat tailward, but the TPA-associated closed flux tubes are simultaneously twisted clockwise (anti-clockwise), depending on the dawnward (duskward) IMF-B_y component during concomitant oppositely-oriented nightside plasma sheet deformation (Tsyganenko et al. 2015; Tsyganenko and Fairfield, 2004), shown by inclined red bars. The closed flux tube twisting is caused by the IMF-B_y penetration, which produces “asymmetry” for the magnetic fields in the Northern and Southern hemisphere, exerting “torque rotation” due to the electromagnetic force (Gosling et al. 1990; Cowley, 1981, 1994). This results in the “L”- and “J”-shaped TPAs, corresponding to the auroral zone footpoints of these field lines in the Northern and Southern hemispheres.

Discussion

In this study, we discover two morphological types of TPAs; “L”- and “J”-shaped TPAs. The main “bar-like” emission of the TPA locates in the dusk (dawn) sector while the TPA nightside ends get distorted toward post-midnight (pre-midnight). We also demonstrate that the formation of the nightside distorted TPA can be explained by electric currents flowing aligned to the magnetic field lines (FACs), induced by plasma flow shear between the fast flows generated by nightside magnetic reconnection and background slow plasma flows. The TPAs grow as the magnetic reconnection points retreat down-tail, which is consistent with the framework of the conventional nightside magnetic reconnection model (Milan et al. 2005). Before and during all nightside distorted TPAs examined in this study (listed in Table S1), the IMF-B_z had been dominantly northward, however magnetotail reconnection appears to occur and, at least, persist during the TPA interval. This result is supported by significant enhancements in geomagnetic activity even under strong and persistent northward IMF-B_z conditions (Shi et al. 2012), and indicates that solar wind energy can enter the magnetosphere during the northward IMF intervals.

The electric current vortices are clear evidence of FACs flowing out of the auroral zone to the magnetotail. However, their scales were found to be different between two nightside distorted TPA intervals; a large-scale vortex was seen at the first interval, and during the second “L”-shaped TPA interval, local small-scale vortices were found at the observatories near the TPA. Because these FACs were induced by the plasma flow shear, the velocity of the plasma flows associated with magnetotail reconnection would be a key physical parameter to determine the current vortex scale on the ground. Therefore, the current vortex scale might be rather proportional to the plasma flow speed. The electric current vortex scale should become smaller, if the energy of plasma (electrons) released by magnetic reconnection in the magnetotail was dissipated upon the auroral zone (Tanskanen et al. 2002).

After the onset of nightside reconnection, the reconnection locations retreated tailward as the TPA approached the dayside, and apparently become "stagnant points", which are unaffected by magnetospheric convection. Furthermore, the closed flux tubes within the nightside distorted TPAs, which are generated by persistent nightside reconnection even under northward IMF conditions, are twisted, associated with the magnetotail deformation. During the nightside distorted TPA, as the reconnection site moves further tailward, the tail deformation becomes larger and associated field lines are also twisted more strongly (Tsyganenko et al. 2015; Tsyganenko and Fairfield, 2004). Significantly, this twisting of field lines, caused by the IMF-B_y penetration (Gosling et al. 1990; Cowley, 1981, 1994), gives opposite chirality to the "J"- and "L"-shaped TPAs seen in the Northern and Southern hemispheres. In previous study (Milan et al. 2005), it has been considered that the nightside magnetospheric deformation and field line twisting are only a phenomenon to determine the TPA growth point in the nightside main auroral oval. Our scenario, however, emphasizes that they play an important role in determining not only the TPA morphology but also how the plasma (electrons) released by magnetotail reconnection are transported to the auroral zone.

Based on this study, we demonstrate that investigations on TPA morphology are important in assessing how the energy stored in the magnetotail, "deformed" by the IMF, is released and transported to the auroral zone. As a result, the nightside distorted TPA is a good remote-sensing diagnostic tool for global magnetospheric effects. The fundamental characteristics and the formation scenario of nightside distorted TPAs obtained through this study have clear potential for application to other planets, and contributes to understanding the influence of the IMF and solar wind plasma on auroral processes at Jupiter, Saturn, and the other planets of solar system. Hereafter, more detailed observations for the solar wind-magnetosphere-auroral zone coupling are required to better understand the process of nightside distorted TPA formation.

Acknowledgments

This work is supported by grants of the National Natural Science Foundation of China (NSFC 41961130382, 41974189, and 41404131). B.H. is supported by the Belgian National Fund for Scientific Research (FNRS). A.W.D is supported by NSFC grant (41774172). A.G. is supported by STFC grant (ST/R000816/1) and NERC grant (NE/P001556/1). M.N. thanks Anthony T. Y. Lui for constructive and insightful discussion on our obtained results, and for modeling of the nightside distorted TPAs, and Chen-Yao Han for helping to draw Figure 6. The SuperDARN radars are funded by the research agencies of Australia, China, Canada, France, Italy, Japan, South Africa, the U. K. and the U. S. For the ground magnetometer data we gratefully acknowledge: Intermagnet; USGS, Jeffrey J. Love; CARISMA, PI Ian Mann; CANMOS, Geomagnetism Unit of the Geological Survey of Canada; The S-RAMP Database, PI K. Yumoto and Dr. K. Shiokawa; The SPIDR database; AARI, PI Oleg Troshichev; The MACCS program, PI M. Engebretson; GIMA; MEASURE, UCLA IGPP and Florida Institute of Technology; SAMBA, PI Eftyhia Zesta; 210 Chain, PI K. Yumoto; SAMNET, PI Farideh Honary; The IMAGE magnetometer network, PI L. Juusola; AUTUMN, PI Martin Connors; DTU Space, PI Anna Willer; South Pole and McMurdo Magnetometer, PI's Louis J. Lanzarotti and Alan T. Weatherwax; ICESTAR; RAPIDMAG; British Artarctic Survey; McMac, PI Dr. Peter Chi; BGS, PI Dr. Susan Macmillan; Pushkov Institute of Terrestrial Magnetism, Ionosphere and Radio Wave Propagation (IZMIRAN); GFZ, PI Dr. Juergen Matzka; MFGI, PI B. Heilig; IGFPAS, PI J. Reda; University of L'Aquila, PI M. Vellante; BCMT, V. Lesur and A. Chambodut; Data obtained in cooperation with Geoscience Australia, PI Marina Costelloe; AALPIP, co-PIs Bob Clauer and Michael Hartinger; SuperMAG, PI Jesper W. Gjerloev; Sodankylä Geophysical Observatory, PI Tero Raita; Polar Geophysical Institute, Alexander Yahnin and Yarolav Sakharov; Geological Survey of Sweden, Gerhard Schwartz; Swedish Institute of Space Physics, Mastoshi Yamauchi; UiT the Arctic University of Norway, Magnar G. Johnsen; Finish Meteorological Institute, PI Kirsti Kauristie.

Data Availability

IMAGE FUV-WIC data can be obtained by contacting the corresponding authors (M.N. and B.H.) or can also be accessed from http://image.gsfc.nasa.gov. SuperDARN data is freely provided for scientific research purposes and can be obtained by contacting the authors (M.N. and A.G.) or any

of the SuperDARN PI research groups (http://www.superdarn.ac.uk). All SuperDARN radar data are processed by the software of fitacf v1.2 and make_grid v1.14.er. OMNI (ACE) IMF and solar wind plasma were obtained from Coordinated Data Analysis Web (https://cdaweb.sci.gsfc.nasa.gov/index.html/), provided by NASA Goddard Flight Space Flight Center (GSFCs) Space Physics Data Facility. The Geotail MGF and CPI data can be taken from Data ARchives and Transmission System (DARTS), provided by Center for Science-satellite Operation and Data Archive (C-SODA) at ISAS/JAXA (http://darts.isas.jaxa.jp/about.html.en). The ground magnetic field data used in this paper can be downloaded from the SuperMAG website (http://supermag.jhuapl.edu/). We also thank World Data Centre for Geomagnetism, Kyoto University for accessing the data of *AU* and *AL* indices from http://wdc.kugi.kyoto-u.ac.jp/index.html.

References

Birn, J., and Hesse, M., The substorm current wedge and field-aligned currents in MHD simulations of magnetotail reconnection, J. Geophys. Res.: Space physics, 96, A2, 1611 – 1618, (1991).

Black, D. I., Cosmic ray effects and faunal extinctions at geomagnetic field reversals, Earth Planet. Sci. Lett. 3, 225–236, (1967).

Chisham, G., Lester, M., Milan, S. E., Freeman, M. P., Bristow, W. A., Grocott, A., McWilliams, K. A., Ruohoniemi, J. M., Yeoman, T. K., Dyson, P. L., Greenwald, R. A., Kikuchi, T., Pinnock, M., Rash, J. P. S., Sato, N., Sofko, G. J., Villain, J.-P., and Walker, A. D. M., A decade of the Super Dual Auroral Radar Network (SuperDARN): Scientific achievements, new techniques and future directions. Surveys in Geophysics, 28(1), 33 – 109, (2007).

Cowley, S. W. H., Magnetospheric asymmetries associated with the y-component of the IMF, Planet. Space Sci., 29, 79 – 96, (1981).

Cowley, S. W. H., Earth's plasma environment: magnetic reconnection and its effect on magnetospheric fields and flows, Philosophical Transaction: Physical Sciences and Engineering, 349, 1690, The Solar-System: A Review of Results from Space Mission (Nov. 15), 237 – 247, (1994).

Cumnock, J. A., Sharber, J. R., Heelis, R. A., Blomberg, L. G., Germany, G. A., Spann, J. F., and Coley, W. R., Interplanetary magnetic field control of theta aurora development, J. Geophys. Res.: Space physics, 107(A7), 1108, (2002).

Fairfield, D. H., Mukai, T., Brittnacher, M., Reeves, G. D., Kokubun, S., Parks, G. K., Nagai, T., Matsumoto, H., Hashimoto, K., Gurnett, D. A., and Yamamoto, T., Earthward flow bursts in the inner magnetotail and their relation to auroral brightenings, AKR intensifications, geosynchronous particle injections and magnetic activity, J. Geophys. Res.: Space physics, 104, A1, 355 – 370, (1999).

Fear, R. C. and Milan, S. E., The IMF dependence of the local time of transpolar arcs: Implications for formation mechanism, J. Geophys. Res.: Space physics, 117(A03213), (2012a).

Fear, R. C. and Milan, S. E. Ionospheric flows relating to transpolar arc formation, J. Geophys. Res.: Space physics, 117, A09230, (2012b).

Frank, L. A., Craven, J. D., Burch, J. L., and Winningham, J. D., Polar views of the Earth's aurora with Dynamics Explorer, Geophys. Res. Lett., 9(9), 1001 – 1004, (1982).

Gjerloev, J. W., The SuperMAG data processing technique, J. Geophys. Res.: Space physics, 117, A09213, (2012).

Glassmeier, K. -H., Hönisch, M., and Untiedt, J., Ground-based and spacecraft observations of traveling magnetospheric convection twin vortices, J. Geophys. Res.: Space physics, 94, 2520–2528, (1989).

Glassmeier, K. -H., Richter, O., Vogt, J., Möbus, P., and Schwalb, A., The Sun, geomagnetic polarity transitions, and possible biospheric effects: review and illustrating model. Int. J. Astrobiol., 8, 147–159, (2009).

Glassmeier, K. -H., and Vogt, J., Magnetic polarity transitions and biospheric effects, Space Sci. Rev., 155, 1-4, 387 – 410, (2010).

Gosling, J. T., Thomsen, M. F., Bame, S. J., Elphic, R. C., and Russell, C. T., Plasma flow reversals at the dayside magnetopause and the origin of asymmetric polar cap convection, J. Geophys. Res.: Space physics, 95(A6), 8073 – 8084, (1990).

Greenwald, R. A., Baker, K. B., Dudeney, J. R., Pinnock, M., Jones, T. B., Thomas, E. C., Villain, J. -P., Cerisier, J. -C., Senior, C., Hanuise, C., Hunsucker, R. D., Sofko, G., Koehler, J., Nielsen, E., Pellinen, R., Walker, A. D. M., Sato, N., and Yamagishi, H., DARN/SuperDARN: A global view of high latitude convection, Space Sci. Rev., 71(1-4), 761 – 796, (1995).

Grocott, A., Cowley, S. W. H., and Sigwarth, J. B., Ionospheric flow during extended intervals of northward but B_Y-dominated IMF, Ann. Geophys., 21(2), 509 – 538, (2003).

Grocott, A., Badman, S. V., Cowley, S. W. H., Yeoman, T. K., and Cripps, P. J., The influence of IMF B_Y on the nature of the nightside high-latitude ionospheric flow during intervals of positive IMF B_Z, Ann. Geophys., 22(5), 1755 – 1764, (2004).

Hasegawa, A., and Sato, T., Generation of Field Aligned Current During Substorm. In: Akasofu SI. (eds) Dynamics of the Magnetosphere. Astrophysics and Space Science Library (A Series of Books on the Recent Developments of Space Science and of General Geophysics and Astrophysics Published in Connection with the Journal Space Science Reviews), 78. Springer, Dordrecht, (1979).

Heppner, J. P., and Maynard, N. C., Empirical high-latitude electric field models, J. Geophys. Res.: Space physics, 92, 4467 – 4489, (1987).

Kaymaz, Z., Siscoe, G., Luhmann, J. G., Fedder, J. A., and Lyon, J. G., Interplanetary magnetic field control of magnetotail field: IMP 8 data and MHD model compared, J. Geophys. Res.: Space physics, 100, A9, 17,163 – 17,172, (1995).

Kullen, A., Brittnacher, M., Cumnock, J. A., and Blomberg, L. G., Solar wind dependence of the occurrence and motion of polar auroral arcs: A statistical study, J. Geophys. Res.: Space physics, 107(A11), 1362, (2002).

Kullen, A., Fear, R. C., Milan, S. E., Carter, J. A., and Karlsson, T., The statistical difference between bending arcs and regular polar arcs, J. Geophys. Res.: Space physics, 120, (2015).

Milan, S. E., Hubert, B., and Grocott, A., Formation and motion of a transpolar arc in response to dayside and nightside reconnection, J. Geophys. Res.: Space physics, 110, A01212, (2005).

Mende, S. B., Heetderks, H., Frey, H. U., Lampton, M., Geller, S. P., Habraken, S., Renotte, E., Jamar, C., Rochus, P., Spann, J., Fuselier, S. A., Gerard, J. -C., Gladstone, R., Murphree, S., and Cogger, L., Far ultraviolet imaging from the IMAGE spacecraft: 1. System design, Space Sci. Rev., 91, 243 – 270, (2000).

Mende, S. B., Heetderks, H., Frey, H. U., Lampton, M., Geller, S. P., Abiad, R., Siegmund, O. H. W., Tremsin, A. S., Spann, J., Dougani, H., Fuselier, S. A., Magoncelli, A. L., Bumala, M. B., Murphree, S., and Trondsen, T., Far ultraviolet imaging from the IMAGE spacecraft: 2. Wideband FUV imaging, Space Sci. Rev., 91, 271 – 285, (2000).

Mende, S. B., Heetderks, H., Frey, H. U., Stock, J. M., Lampton, M., Geller, S. P., Abiad, R., Siegmund, O. H. W., Habraken, S., Renotte, E., Jamar, C., Rochus, P., Gerard, J. -C., Sigler, R., and Lauche, H., Far ultraviolet imaging from the IMAGE spacecraft: 3. Spectral imaging of Lyman-α and OI 135.6 nm, Space Sci. Rev., 91, 287 – 318, (2000).

Nishida, A., Mukai, T., Yamamoto, T., Saito, Y., Kokubun, S., and Maezawa, K., GEOTAIL observation of magnetospheric convection in the distant tail at 200 R_E in quiet times, J. Geophys. Res.: Space physics, 100, A12, 23,663 – 23,675, (1995).

Nishida, A., Mukai, T., Yamamoto, T., Kokubun, S., and Maezawa, K., A unified model of the magnetotail convection in geomagnetically quiet and active times J. Geophys. Res.: Space physics, 103, A3, 4409 – 4418, (1998).

Nowada, M., Fear, R. C., Grocott, A., Shi, Q. -Q., Yang, J., Zong, Q. -G., Wei, Y., Fu, S. -Y., Pu, Z. -Y., Mailyan, B., and Zhang, H., Subsidence of ionospheric flows triggered by magnetotail magnetic reconnection during transpolar arc brightening, J. Geophys. Res.: Space physics, 123, (2018).

Pitkänen, T., Hamrin, M., Norqvist, P., Karlsson, T., and Nilsson, H., IMF dependence of the azimuthal direction of earthward magnetotail fast flows, Geophys. Res. Lett., 40, 5598, (2013).

Pitkänen, T., Hamrin, M., Norqvist, P., Karlsson, T., Nilsson, H., Kullen, A., Imber, S. M., and Milan, S. E., Azimuthal velocity shear within an earthward fast flow: Further evidence for magnetotail untwisting, Ann. Geophys., 33, 245, (2015).

Pitkänen, T., Hamrin, M., Karlsson, T., Nilsson, H., and Kullen, A., On IMF By-induced dawn-dusk asymmetries in earthward convective fast flows. In S. Haaland, A. Runov, & C. Forsyth (Eds.), Dawn-dusk asymmetries in planetary plasma environments, Geophyscial Monograph Series, 95–106, Hoboken, NJ: John Wiley, (2017).

Ruohoniemi, J. M., and Baker, K. B., Large-scale imaging of high-latitude convection with Super Dual Auroral Radar Network HF radar observations, J. Geophys. Res.: Space physics, 103(A9), 20797 – 20811, (1998).

Ruohoniemi, J. M., and Greenwald, R. A., Statistical patterns of high-latitude convection obtained from Goose Bay HF radar observations, J. Geophys. Res.: Space physics, 101(A10), 21743 – 21763, (1996).

Shi, Q. -Q., Zong, Q. -G., Fu, S. -Y., Dunlop, M. W., Pu, Z. -Y., Parks, G. K., Wei, Y., Li, W. -H., Zhang, H., Nowada, M., Wang, Y. B., Sun, W. -J., Xiao, T., Rème, H., Carr, C., Fazakerley, A. N., and Lucek, E., Solar wind entry into the high-latitude terrestrial magnetosphere during geomagnetically quiet times. Nat. Commun., 4, 1466, (2013).

Shi, X. -F., Zong, Q. -G., and Wang, Y. -F., Comparison between the ring current energy injection and decay under southward and northward IMF B_z conditions during geomagnetic storms, Sci. China Tech, Sci., 55, 10, 2769 – 2777, (2012).

Tanskanen, E., Pulkkinen, T. I., Koskinen, H. E. J., and Slavin, J.A., Substorm energy budget during low and high solar activity: 1997 and 1999 compared, J. Geophys. Res.: Space Physics, 107(A6), 1086, (2002).

Tenfjord, P., Østgaard, N., Snekvik, K., Laundal, K. M., Reistad, J. P., Haaland, S., and Milan, S. E., How the IMF B_y induces a B_y component in the closed magnetosphere and how it leads to asymmetric currents and convection patterns in the two hemispheres, J. Geophys. Res.: Space Physics, 120, 9368 – 9384, (2015).

Tenfjord, P., Østgaard, N., Haaland, S., Snekvik, K., Laundal, K. M., Reistad, J. P., Strangeway, R., Milan, S. E., Hesse, M., and Ohma, A., How the IMF B_y induces a local By component during northward IMF B_z and characteristic timescales, J. Geophys. Res.: Space physics, 123, (2018).

Tsyganenko, N. A., Andreeva, V. A., and Gordeev, E. I., Internally and externally induced deformations of the magnetospheric equatorial current as inferred from spacecraft data, Ann. Geophys., 33, 1 – 11, (2015).

Tsyganenko, N. A., and Fairfield, D. H., Global shape of the magnetotail current sheet as derived from Geotail and Polar data, J. Geophys. Res.: Space physics, 109(A03218), (2004).

Tsyganenko, N. A., and Sitnov, M. I., Modeling the dynamics of the inner magnetosphere during strong geomagnetic storms, J. Geophys. Res.: Space physics, 110 (A3), A03208, (2005).

Wei, Y., Pu, Z. -Y., Zong, Q. -G., Wan, W.-X., Ren, Z. -P., Fraenz, M., Dubinin, E., Tian, F., Shi, Q. -Q., Fu, S. -Y., Hong, M. -H., Oxygen escape from the Earth during geomagnetic reversals: Implications to mass extinction, Earth Planet. Sci. Lett., 394, 94-98, (2014).

Figures and Captions

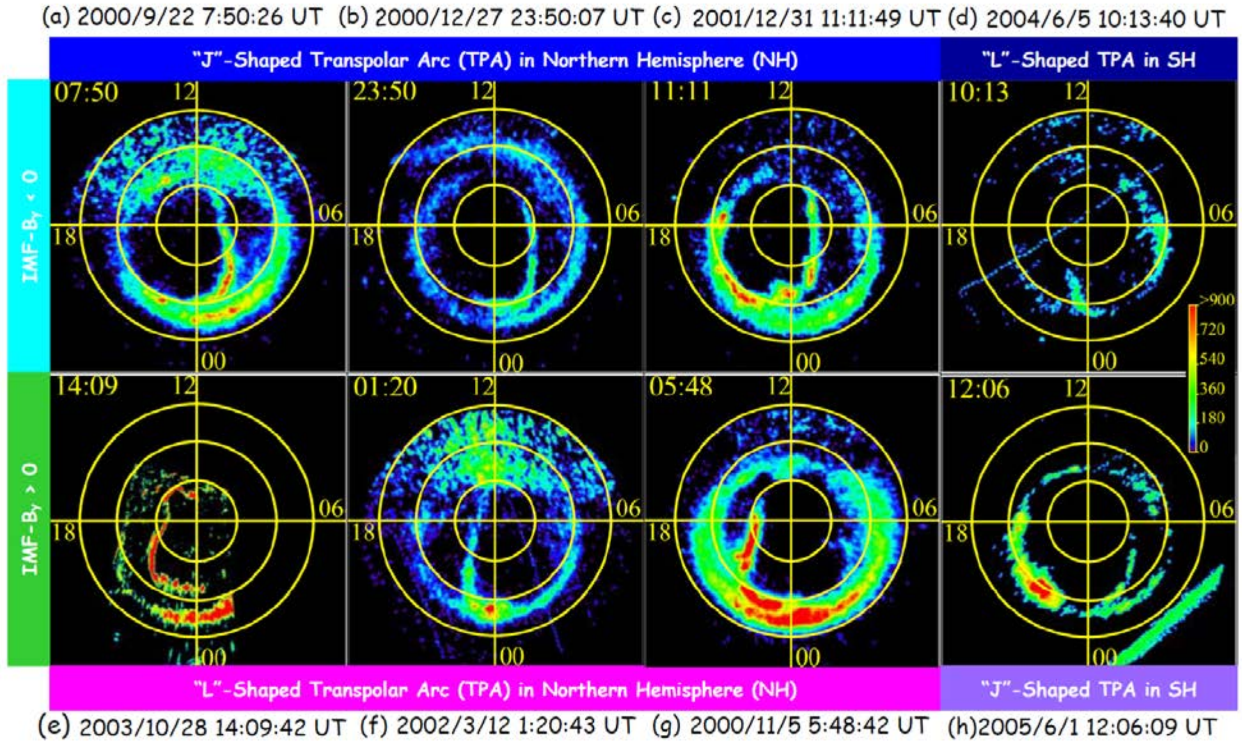

Figure 1: IMAGE-FUV-WIC data plots of selected 8 nightside distorted TPAs are shown. The upper panels (a) to (c) display the "J"-shaped TPAs whose nightside ends are distorted toward midnight or pre-midnight, observed in the Northern Hemisphere under negative (dawnward) IMF-B_y conditions. Panels (e) to (g) show the "L"-shaped TPAs with the nightside ends distorted toward midnight or post-midnight during positive (duskward) IMF-B_y intervals. Panels (d) and (h) show an "L"-shaped, and a "J"-shaped TPAs in the Southern Hemisphere during negative and positive IMF-B_y intervals. These panels are orientated in the same way, with noon (midnight) at the top (bottom), and dusk (dawn) on the left (right) of each plot. The yellow concentric circles show the magnetic latitude (MLat) from 60 degrees to 80 degrees. The color code is assigned according to Analogic-Digital Units (ADU), which is comparable to a detector count rate, being proportional to the observed auroral brightness (accounting for the spectral response of the instrument).

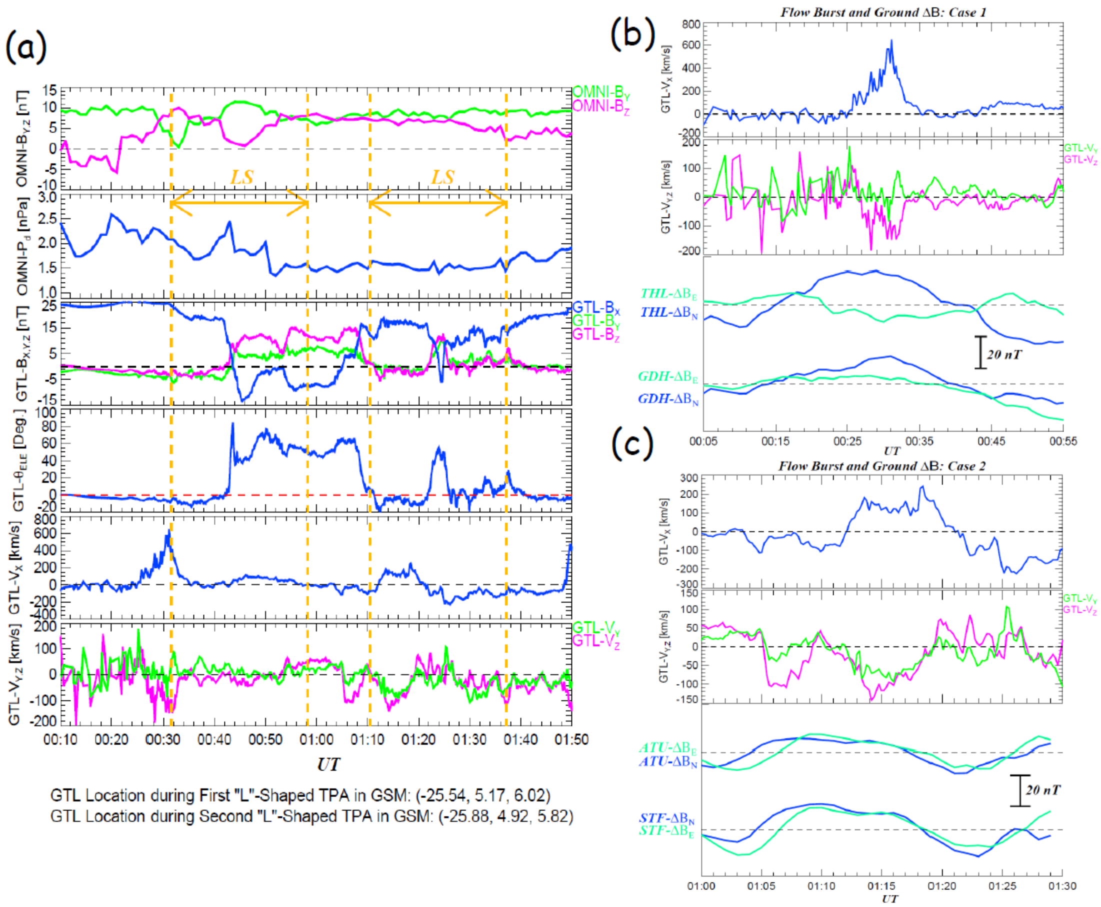

Figure 2: The summary plots of in-situ solar wind, duskside magnetotail and corresponding ground-based magnetic field observations on 12^{th} March 2002 are displayed. Panel (a) shows a summary plot of OMNI-solar wind and Geotail magnetic field and plasma data in the duskside magnetotail during a 1 h 40 minute interval from 0:10 UT to 1:50 UT on 12^{th} March 2002. The panels from top to bottom show the IMF-B_y and -B_z components in GSM coordinates, solar wind dynamic pressure, the three components of the duskside magnetotail magnetic field in GSM, associated magnetic field elevation angle, and the three components of plasma velocity in the duskside magnetotail in GSM coordinates, respectively. Two "L"-shaped TPA intervals are bracketed with two gold broken lines. Zoomed-in three plasma flow velocity components in GSM, including significant V_x enhancements which suggest an earthward plasma flow burst, and corresponding geomagnetic field variations observed at two representative ground observatories close to the "L"-shaped TPAs are shown in panels (b) and (c). The geomagnetic field fluctuations are calculated by a subtraction of the magnetic field average during the presented interval from the observed magnetic field data.

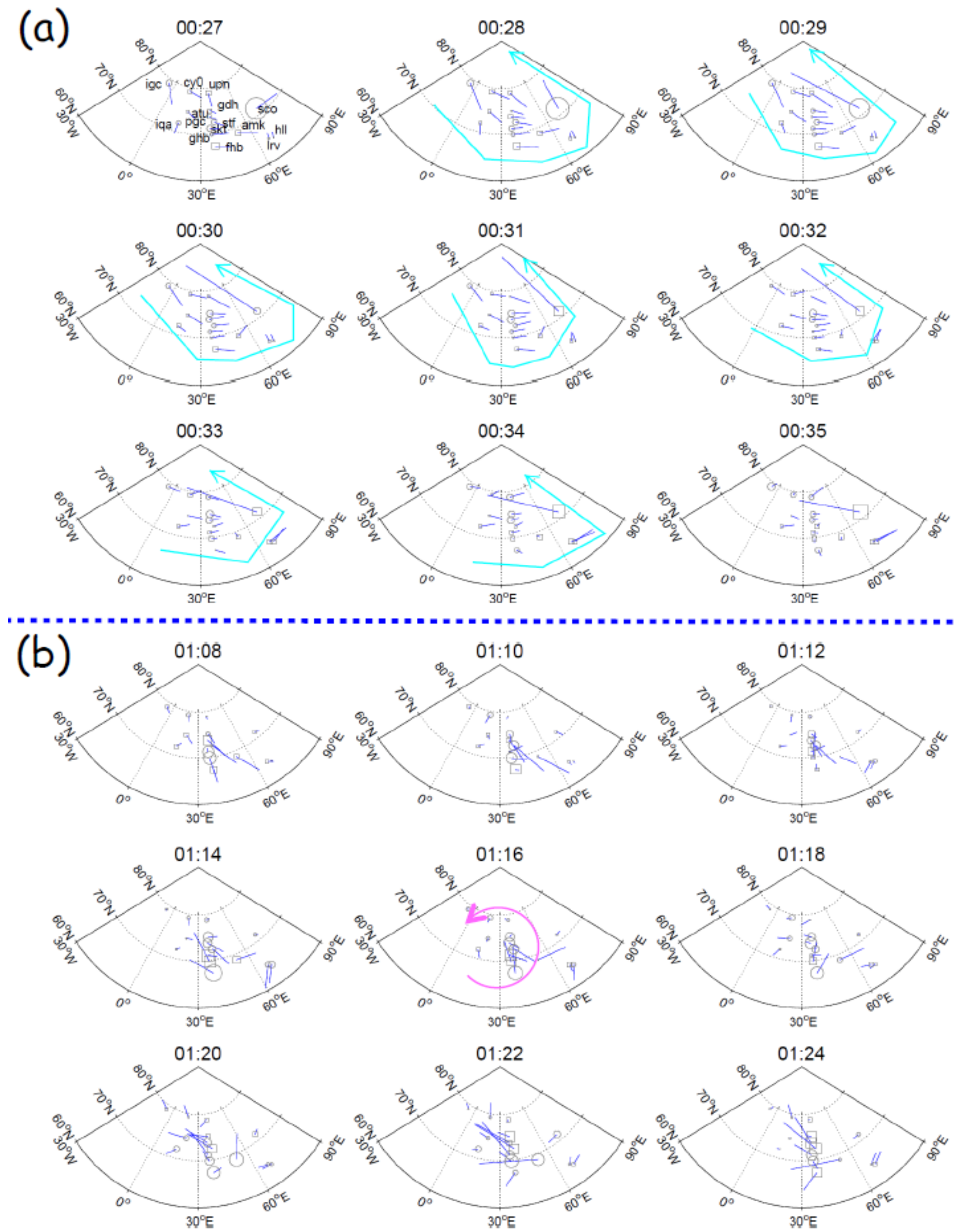

Figure 3: The electric current vortex-like structures detected by ground magnetic observatories beneath and in close proximity to the growth region of the "L"-shaped TPA on 12th March 2002 are shown. The electric current vectors are derived based on the ground magnetic field fluctuations during the time intervals including the first (a) and second (b) plasma earthward flow bursts, projected onto geomagnetic coordinates. Squares and circles with different sizes denote the polarity (positive and negative) and scale of the vertical directional magnetic field fluctuation component (ΔB_Z). Cyan and magenta circle arrows denote large- and small-scale anti-clockwise current vortices, respectively.

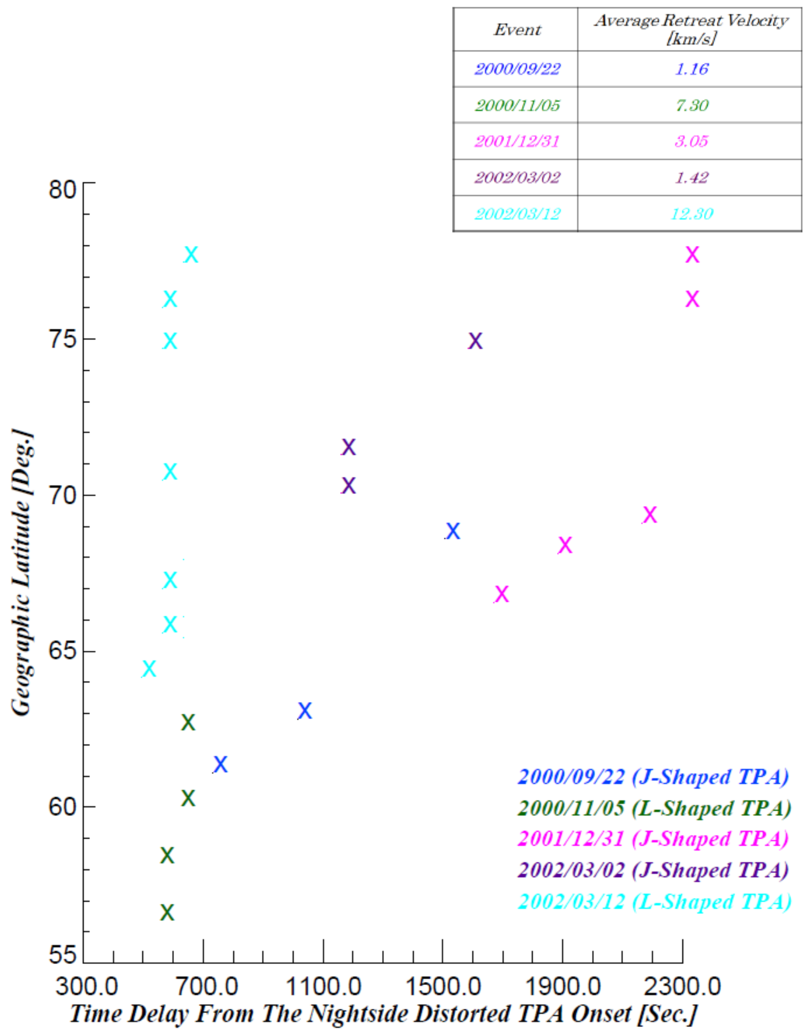

Figure 4: The relationship between the magnetic peaks observed at several ground observatories beneath and in close proximity to the growth regions of the 5 nightside distorted TPAs from geographical low- to high-latitudes, and the time delays from the 5 TPA onset times to the magnetic peak times is shown. The magnetic field peaks seen in the local magnetic north-south magnetic field component (ΔB_N) are used. The rough estimation result of the reconnection point retreat speed, which was calculated using the values of the time delay and 1 degree = 110.95 km in geographical latitude, is summarized in the table on the top in the right side.

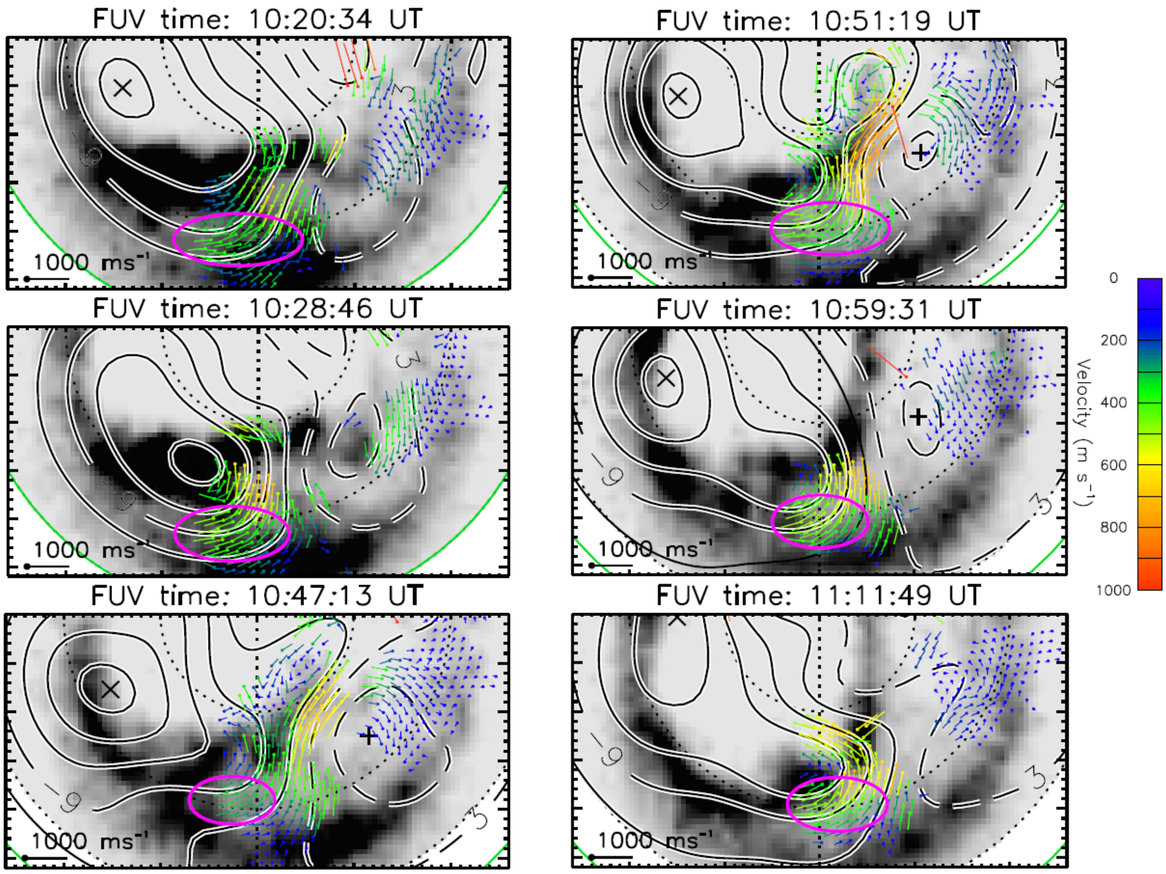

Figure 5: The nightside polar cap plasma flow streamlines and their line-of-sight velocity vectors measured by SuperDARN in the northern hemisphere, overlaid by the IMAGE FUV-WIC auroral image data, are shown. The dotted circles indicate the magnetic latitude (MLat) from 60 degrees to 80 degrees. The left, bottom and right sides in each panel show 18h, 24h and 6h in magnetic local time (MLT), respectively. The time resolutions of the SuperDARN and IMAGE FUV-WIC data are 2 minutes. These streamlines and velocity vectors are projected onto the geomagnetic grids, and positive (maximum denoted by a plus) and negative (minimum shown with a cross) electrostatic potential models, which are controlled by the IMF conditions, as shown with black solid and broken contours on dawn and dusk. The equipotential values are also overlaid. The green curves show the lower latitude limit of the plasma convection pattern in the polar cap (Heppner and Maynard, 1987), determined from the line-of-sight plasma velocities measured by the radars. Each dot shows a SuperDARN radar measurement. The length of the vectors and color code are assigned according to the flow orientation and speed in units of m/s. Westward "Tail Reconnection during IMF Northward and Non-substorm Interval" (TRINNI) flows are marked with magenta ovals.

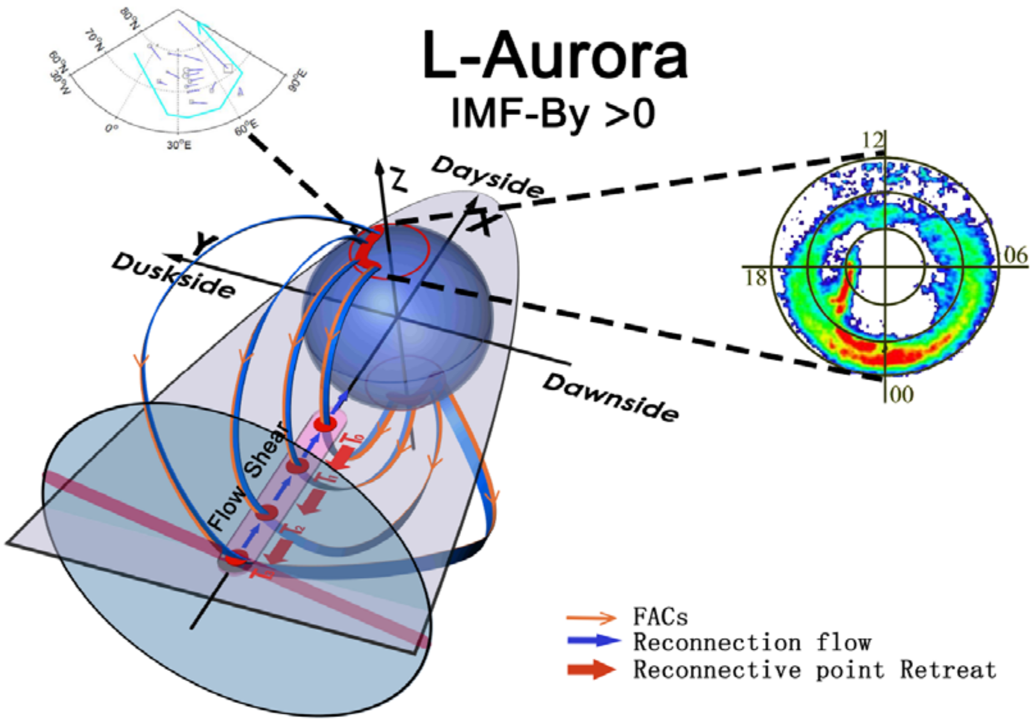

Figure 6: A schematic illustration showing a possible scenario for the formation of nightside distorted TPAs in terms of the magnetic field configuration changes, field-aligned currents (FACs), the magnetic reconnection plasma flows and the reconnection point retreats is shown. This illustration includes the observational examples of the "L"-shaped TPA, obtained by the IMAGE FUV-WIC on November 5th, 2000, and the counter-clockwise current vortex, induced by FACs flowing out of the auroral zone. The magnetotail cross section and twisted plasma sheet are shown with a gray-shaded circle and red bar, respectively. FACs flowing toward magnetotail are indicated by orange curved arrows, and thin blue arrows show the fast plasma flows generated by magnetotail magnetic reconnection. The progressive retreat profile of the reconnection points (red dots) from T_0 to T_3 is shown with thick red arrows.

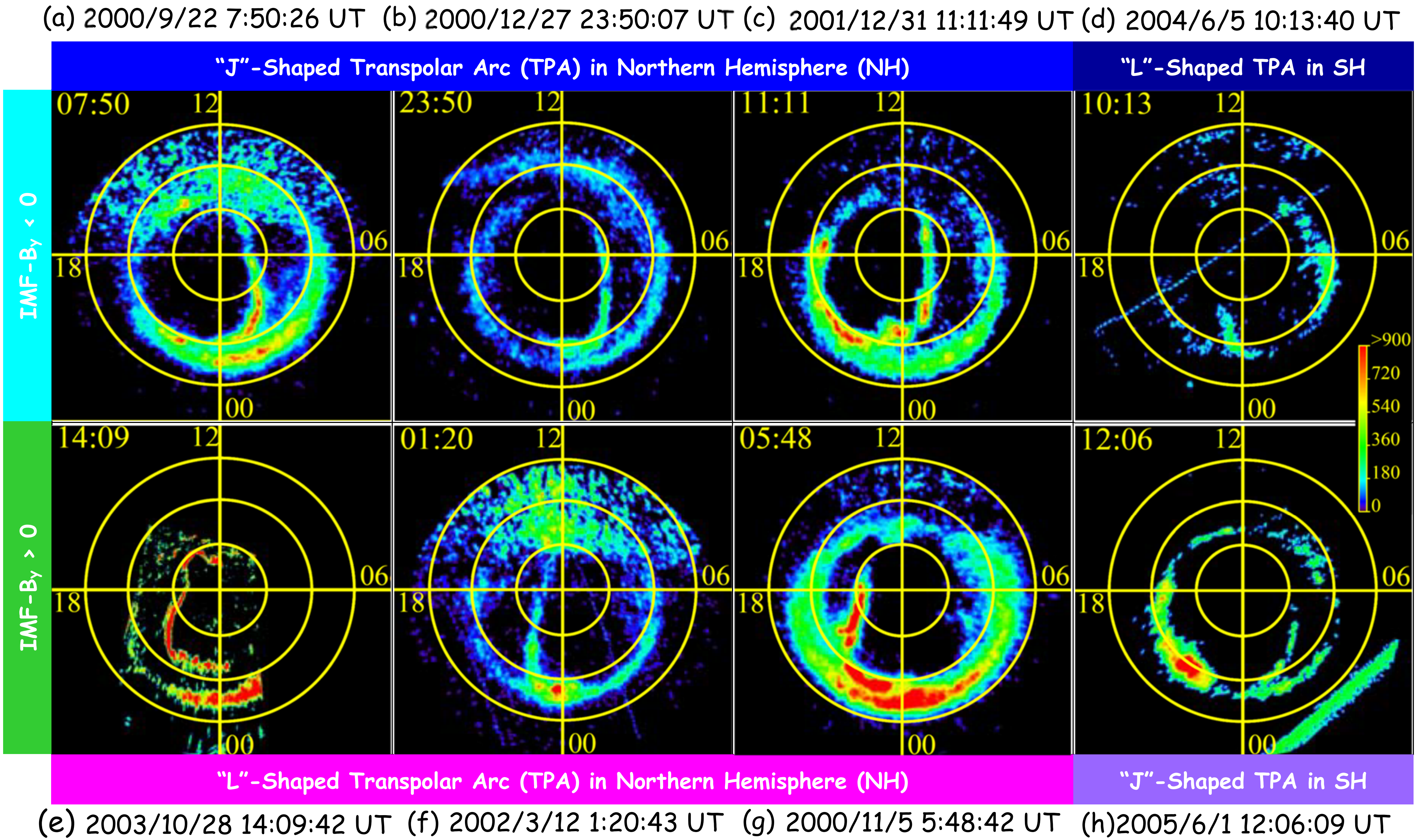

(a) 2000/9/22 7:50:26 UT (b) 2000/12/27 23:50:07 UT (c) 2001/12/31 11:11:49 UT (d) 2004/6/5 10:13:40 UT
"J"-Shaped Transpolar Arc (TPA) in Northern Hemisphere (NH)
"L"-Shaped TPA in SH
IMF-By < 0
IMF-By > 0
07:50
23:50
11:11
10:13
14:09
01:20
05:48
12:06
12
06
18
00
>900
720
540
360
180
0
"L"-Shaped Transpolar Arc (TPA) in Northern Hemisphere (NH)
"J"-Shaped TPA in SH
(e) 2003/10/28 14:09:42 UT (f) 2002/3/12 1:20:43 UT (g) 2000/11/5 5:48:42 UT (h)2005/6/1 12:06:09 UT

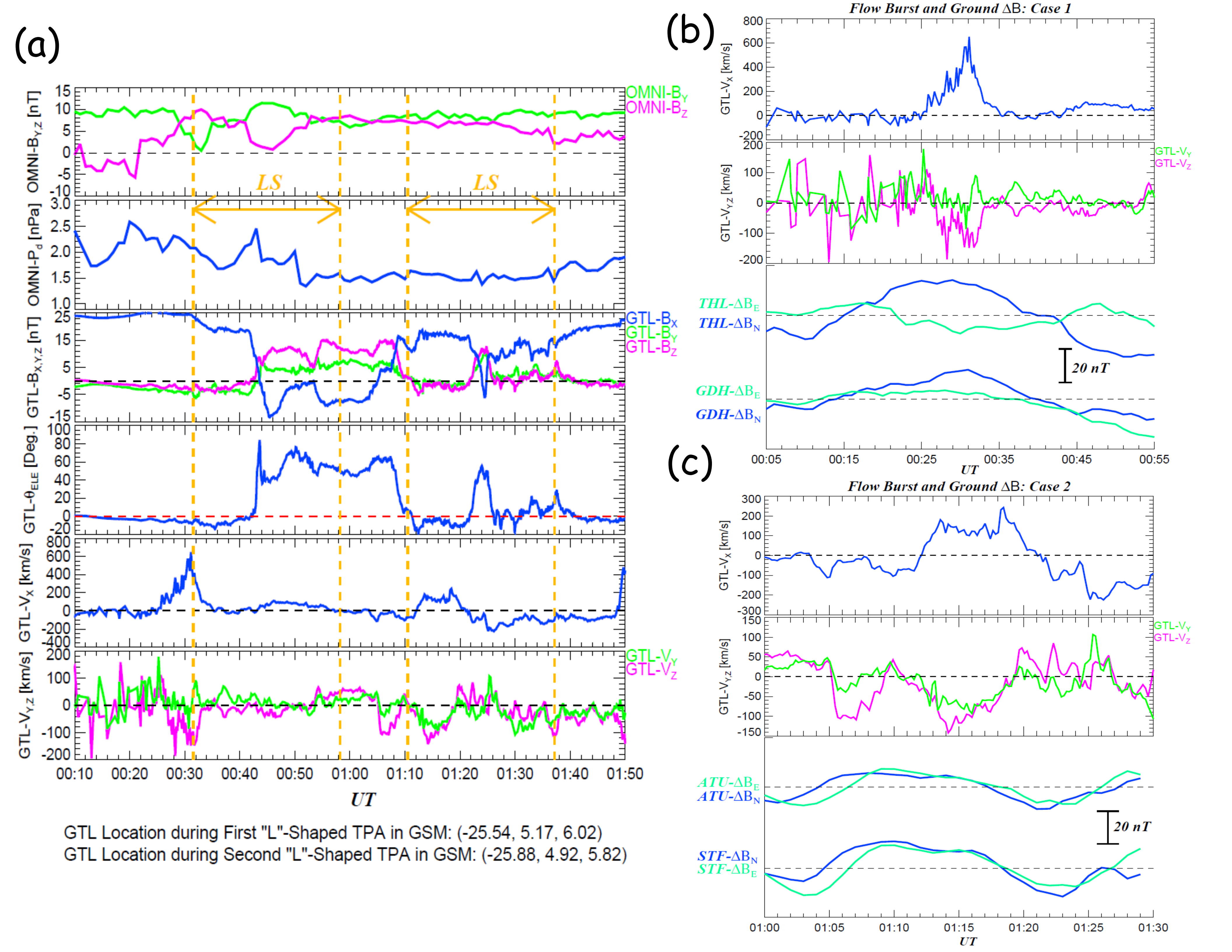
(a)
OMNI-B$_Y$
OMNI-B$_Z$
OMNI-B$_{Y,Z}$ [nT]
LS
LS
OMNI-P$_d$ [nPa]
GTL-B$_X$
GTL-B$_Y$
GTL-B$_Z$
GTL-B$_{X,Y,Z}$ [nT]
GTL-θ$_{ELE}$ [Deg.]
GTL-V$_X$ [km/s]
GTL-V$_Y$
GTL-V$_Z$
GTL-V$_{Y,Z}$ [km/s]
00:10 00:20 00:30 00:40 00:50 01:00 01:10 01:20 01:30 01:40 01:50
UT
GTL Location during First "L"-Shaped TPA in GSM: (-25.54, 5.17, 6.02)
GTL Location during Second "L"-Shaped TPA in GSM: (-25.88, 4.92, 5.82)
(b)
Flow Burst and Ground ΔB: Case 1
GTL-V$_X$ [km/s]
GTL-V$_Y$
GTL-V$_Z$
GTL-V$_{Y,Z}$ [km/s]
THL-ΔB$_E$
THL-ΔB$_N$
20 nT
GDH-ΔB$_E$
GDH-ΔB$_N$
00:05 00:15 00:25 00:35 00:45 00:55
UT
(c)
Flow Burst and Ground ΔB: Case 2
GTL-V$_X$ [km/s]
GTL-V$_Y$
GTL-V$_Z$
GTL-V$_{Y,Z}$ [km/s]
ATU-ΔB$_E$
ATU-ΔB$_N$
20 nT
STF-ΔB$_N$
STF-ΔB$_E$
01:00 01:05 01:10 01:15 01:20 01:25 01:30
UT

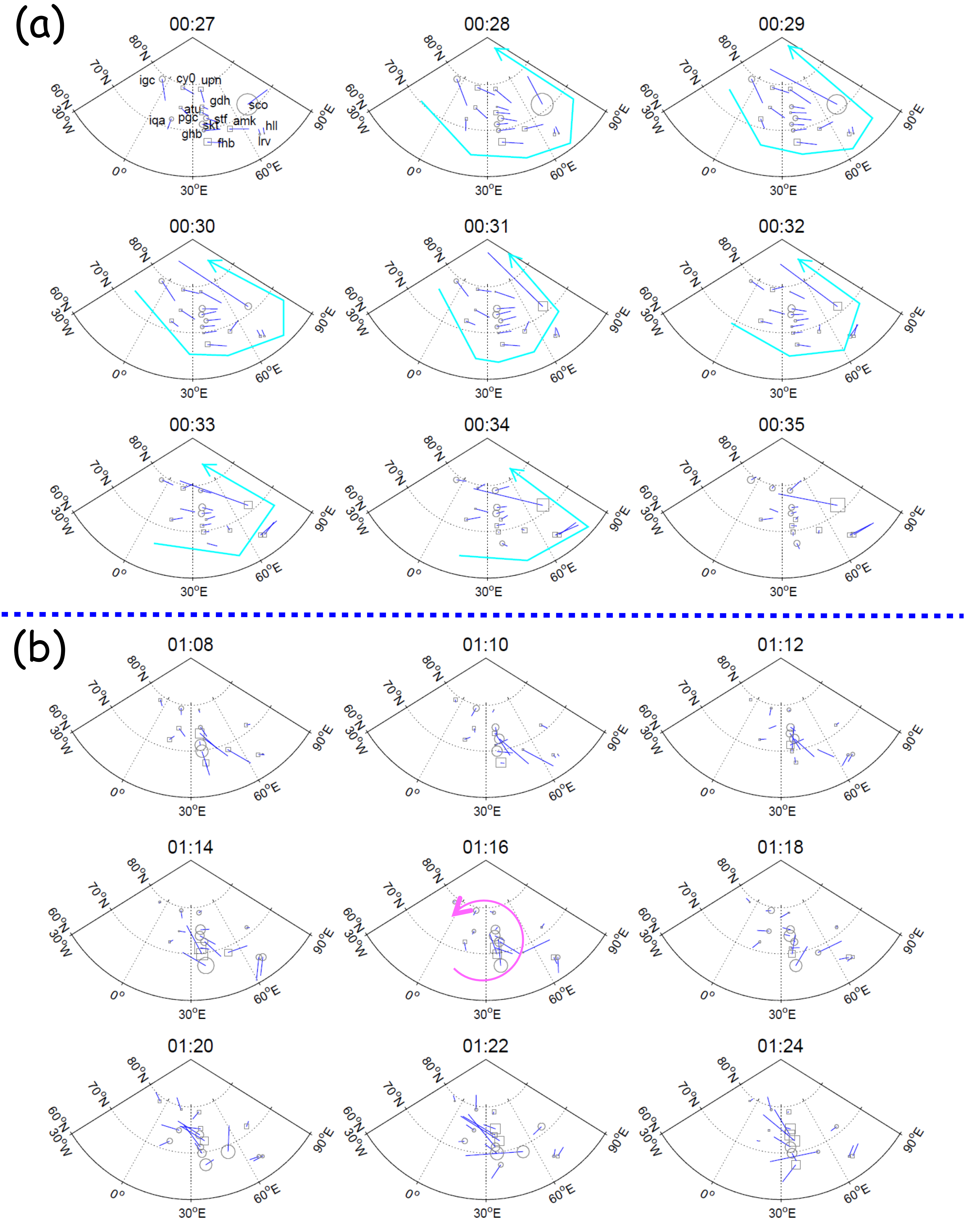
(a)
00:27
00:28
00:29
00:30
00:31
00:32
00:33
00:34
00:35
igc
cy0
upn
gdh
sco
atu
pgc
iqa
stf
amk
hll
skt
ghb
fhb
lrv
80°N
70°N
60°N
30°W
0°
30°E
60°E
90°E
(b)
01:08
01:10
01:12
01:14
01:16
01:18
01:20
01:22
01:24

Event	Average Retreat Velocity [km/s]
2000/09/22	1.16
2000/11/05	7.30
2001/12/31	3.05
2002/03/02	1.42
2002/03/12	12.30

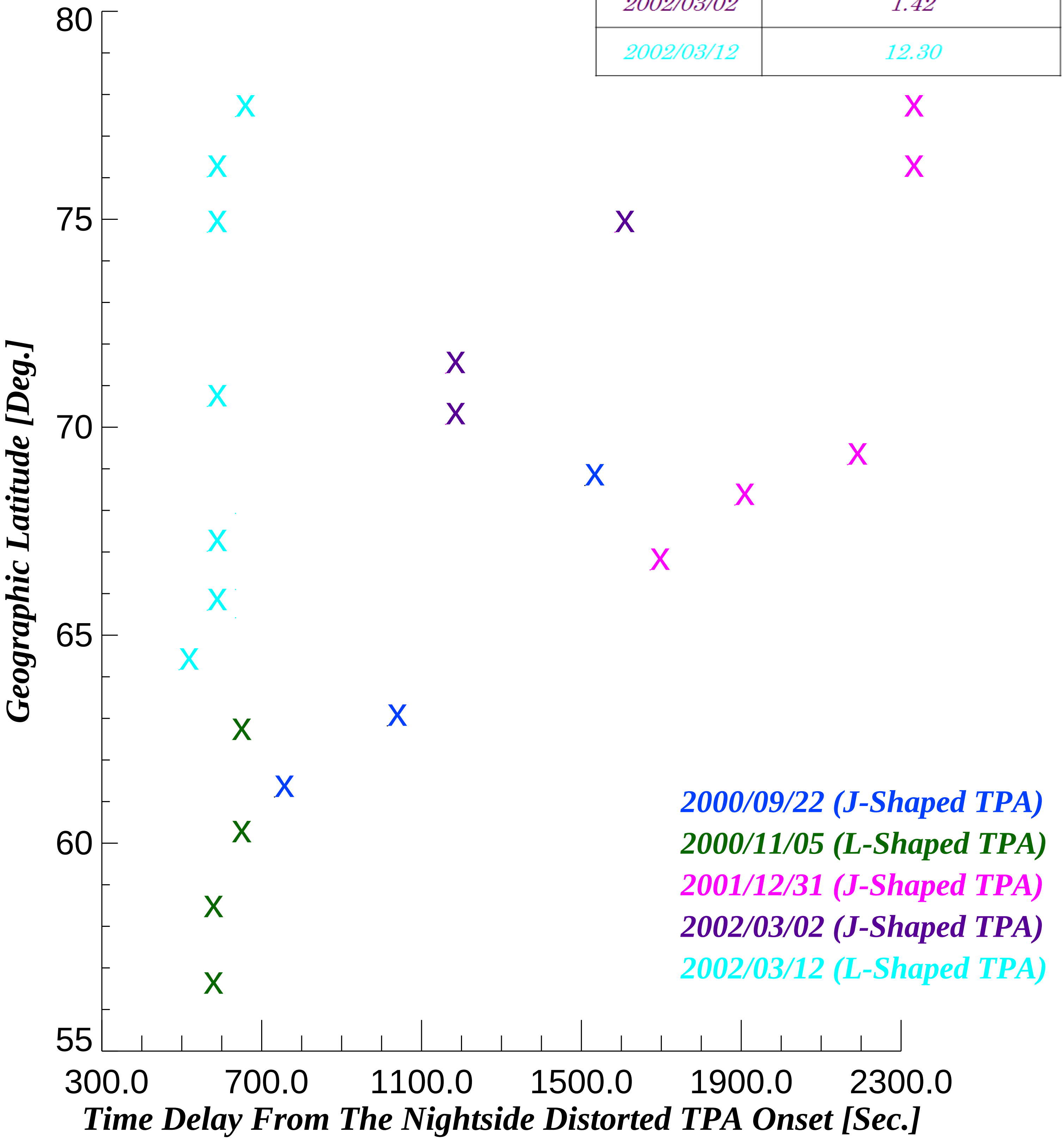

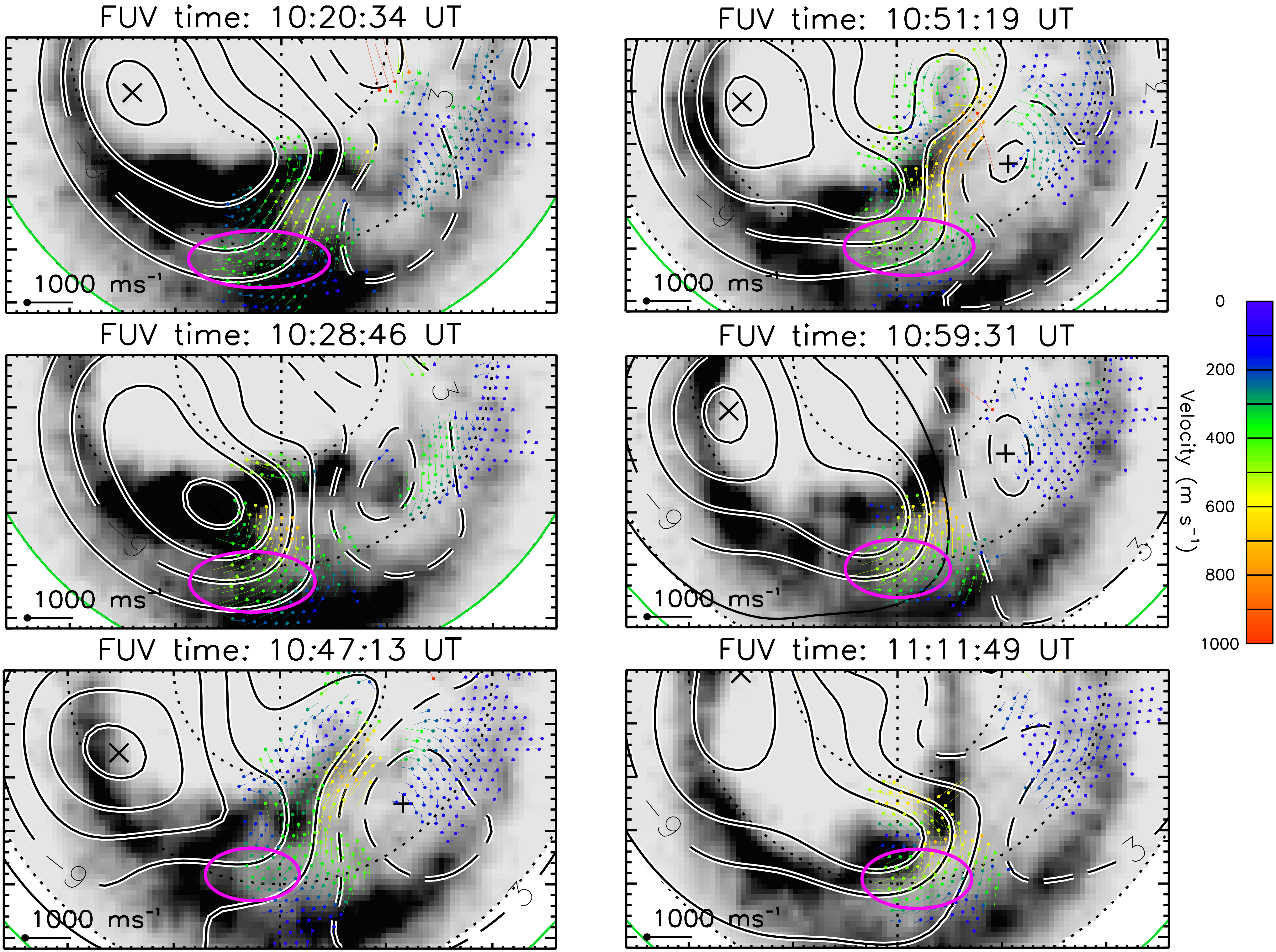
FUV time: 10:20:34 UT
FUV time: 10:51:19 UT
FUV time: 10:28:46 UT
FUV time: 10:59:31 UT
FUV time: 10:47:13 UT
FUV time: 11:11:49 UT
1000 ms^{-1}
-9
3
Velocity (m s^{-1})
0
200
400
600
800
1000

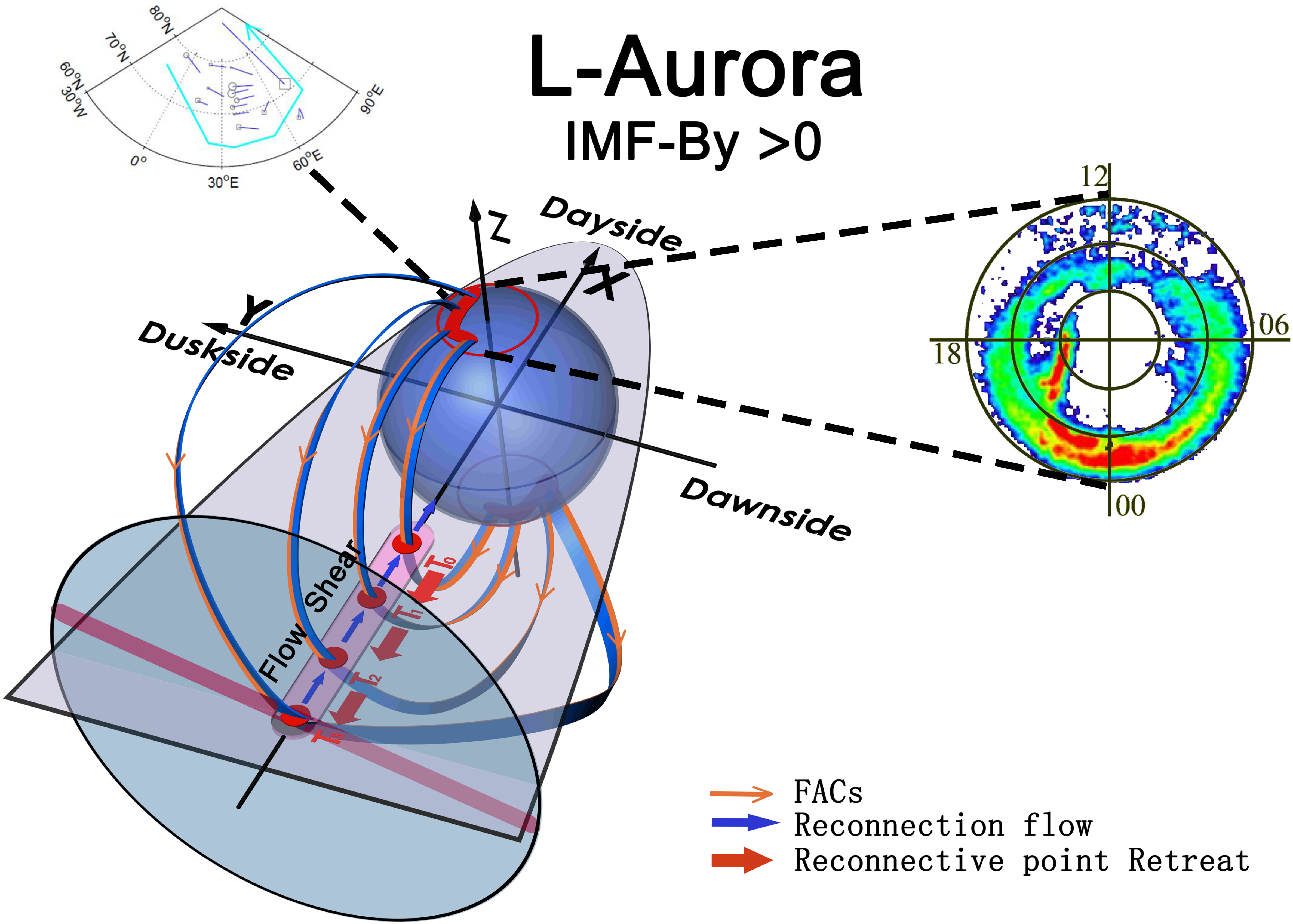

L-Aurora
IMF-By >0
80°N
70°N
60°N
30°W
0°
30°E
60°E
90°E
12
06
18
00
Z
X
Y
Dayside
Duskside
Dawnside
Flow Shear
T0
T1
T2
T3
FACs
Reconnection flow
Reconnective point Retreat

Journal of Geophysical Research: Space Physics

Supporting Information for

Plasma Transport Process from A Deformed Magnetotail to The High-latitude Atmosphere Manifested by A Nightside Distorted Auroral Transpolar Arc

Motoharu Nowada[1], Qiu-Gang Zong[2], Benoît Hubert[3], Quan-Qi Shi[1], Yong-Fu Wang[2], Jun Yang[1], Adrian Grocott[4], Alexander W. Degeling[1], An-Min Tian[1], Xu-Zhi Zhou[2], and Chao Yue[2]

1. Shandong Provincial Key Laboratory of Optical Astronomy and Solar-Terrestrial Environment, Institute of Space Sciences, Shandong University, Weihai, People's Republic of China.

2. Institute of Space Physics and Applied Technology, School of Earth and Space Sciences, Peking University, People's Republic of China.

3. Space science, Technologies and Astrophysics Research (STAR) Institute, Université de Liège, Belgium.

4. Space and Planetary Physics Group, Department of Physics, Lancaster University, Lancaster, UK.

Contents of this file

Introduction

The 5 auroral imager snapshots of the temporal evolutions of the 4 nightside distorted TPAs and corresponding IMF and solar wind plasma conditions are shown in Figure S1. The IMF and solar wind plasma parameters were obtained through the measurements of ACE and Geotail. In the auroral imager data, the optical noises such as the dayglow contaminations were removed using the same techniques as the noise removals in the auroral imager data shown in Figure 1. Figure S2 shows the plots of the magnetic field and plasma data taken from the Geotail measurements of the dawnside magnetotail on March 2nd, 2002, corresponding solar wind conditions, and the geomagnetic field perturbations measured at two representative ground magnetic observatories close to the "J"-shaped TPA. The plots of in-situ geomagnetic magnetic field variations beneath and in close proximity to the regions of growth of the 5 nightside distorted TPAs are displayed in Figure S3.

2000/9/22 6:34:53 UT – 8:25:08 UT (IMAGE-FUV-WIC)

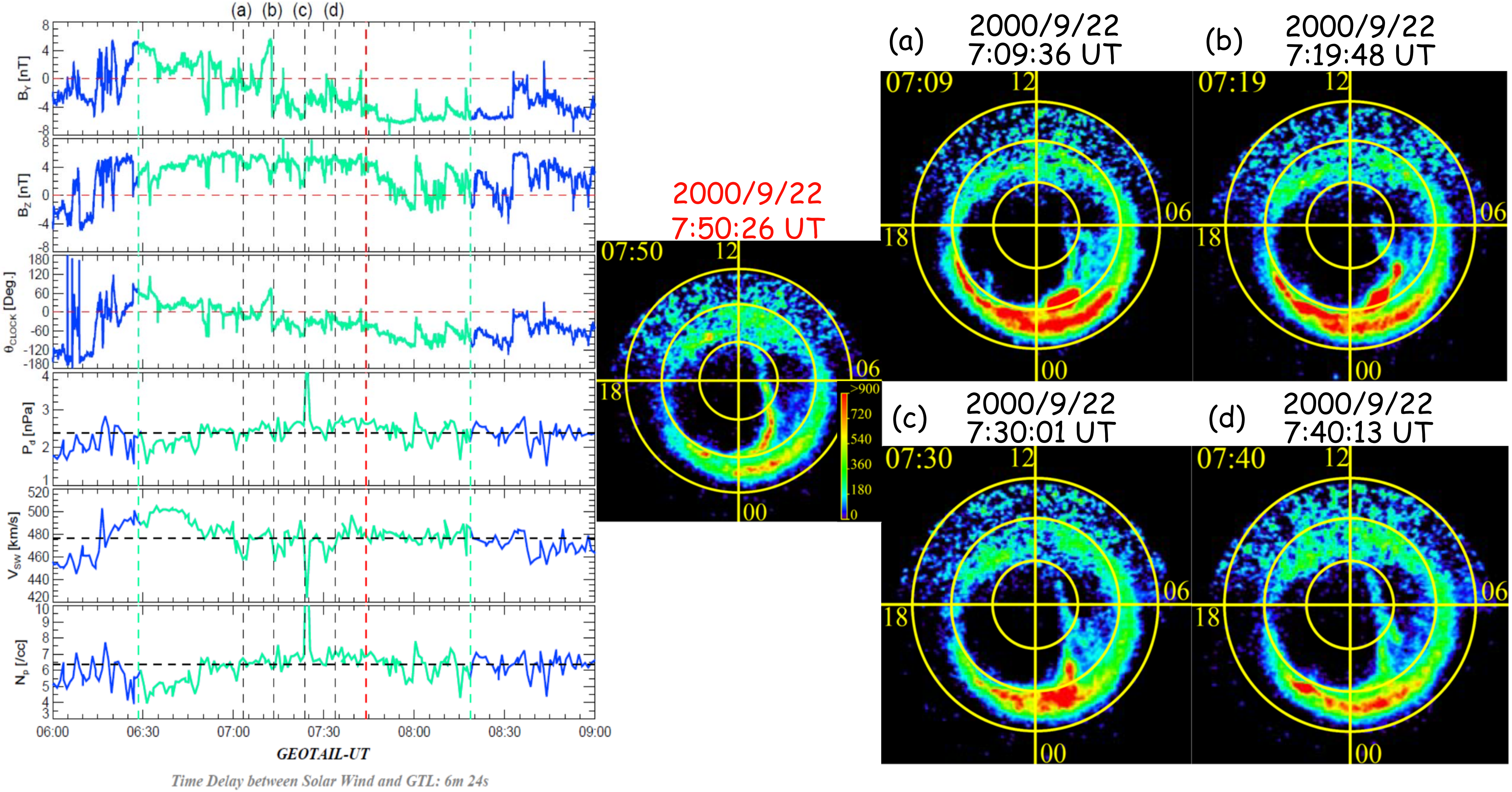

2000/11/5 5:34:24 UT – 7:08:24 UT (IMAGE-FUV-WIC)

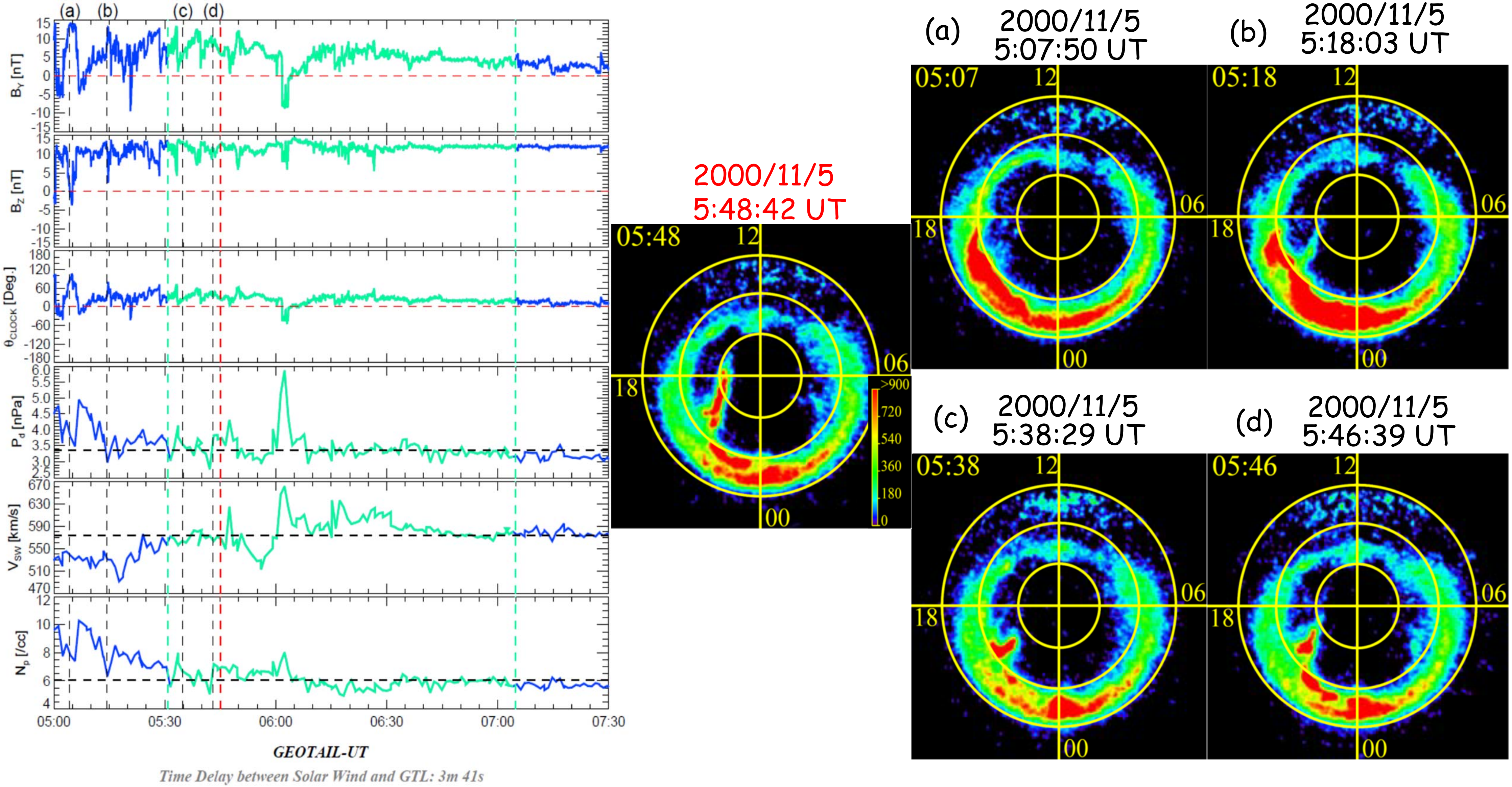

2001/12/31 10:20:34 UT – 14:40:46 UT (IMAGE-FUV-WIC)

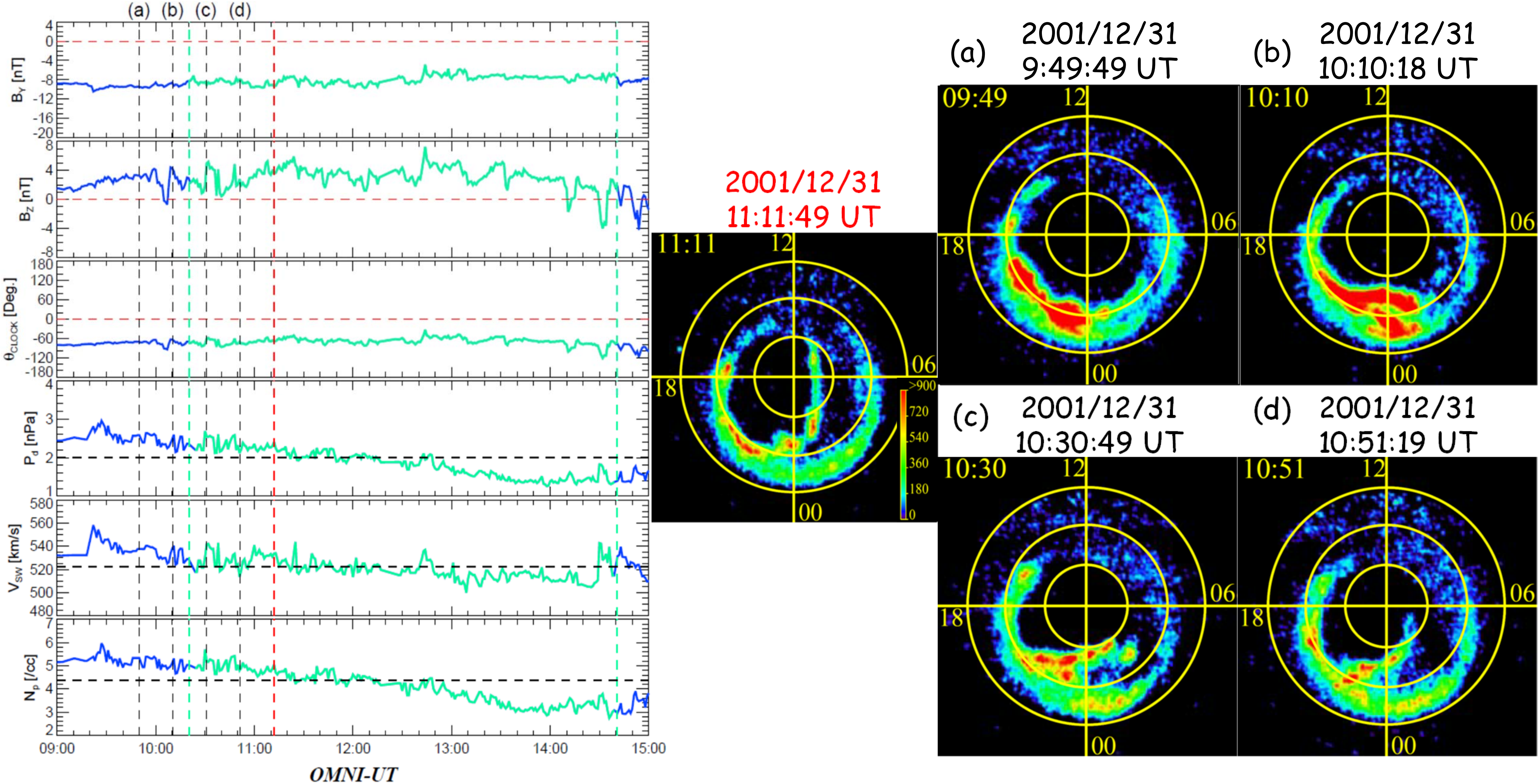

2003/10/28 13:20:28 UT – 14:17:55 UT (IMAGE-FUV-WIC)

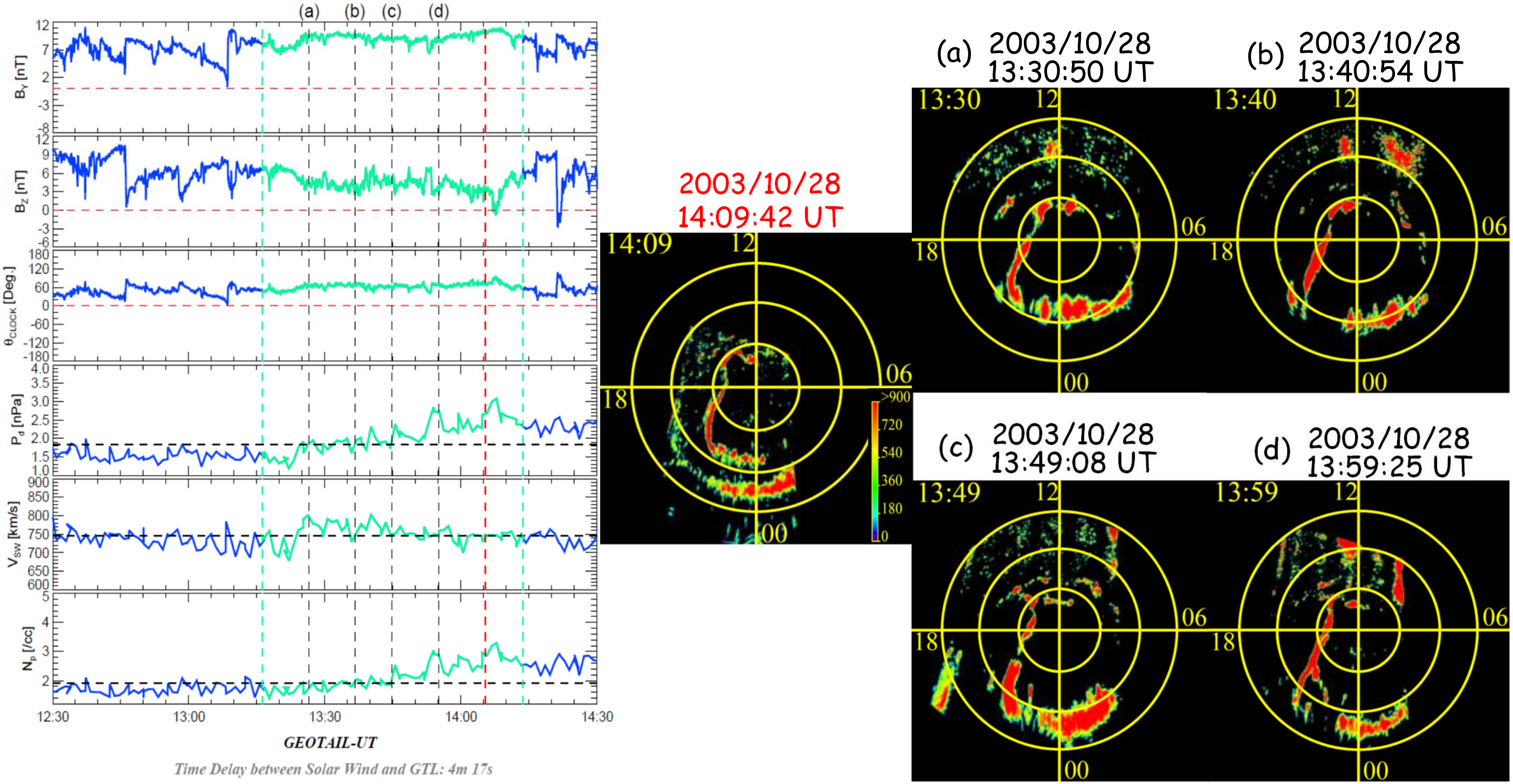

Figure S1. The 5 auroral imager snapshots of evolutional time sequence of the nightside distorted TPAs (right) and corresponding solar wind conditions (left) obtained from the OMNI solar wind database and the Geotail solar wind measurements are displayed. The "J"- and "L"-shaped TPA events observed on September 22nd, 2000 and November 5th, 2000 are shown in Figures S1A and S1B. Figures S1C and S1D display another "J"- and "L"-shaped TPA cases seen on December 31st, 2001 and October 28th, 2003, respectively. The plots of solar wind conditions show the IMF-B_y and -B_z components in GSM coordinates, IMF clock angle, calculated by $\tan^{-1}$(IMF-B_y/IMF-B_z), solar wind dynamic pressure ($P_d = m_p N_p V_{sw}^2$), when solar wind ion species are assumed as protons, solar wind velocity and number density, respectively. The nightside distorted TPA intervals are plotted with light green and also bracketed by two light green broken lines. The black vertical broken lines, labelled from (a) to (d), correspond to the solar wind conditions at the times when the IMAGE FUV-WIC data from (a) to (d) shown in right column were obtained. The times when IMAGE FUV-WIC detected the clear "J"- and "L"-shaped TPA cases (middle) are highlighted with red, and associated solar wind conditions are indicated with red vertical broken lines. The IMAGE FUV-WIC data plot formats from Figures S1A to S1D are the same as that of Figure 1. The time delay between the solar wind and spacecraft location is indicated below the panels in the Geotail observational cases.

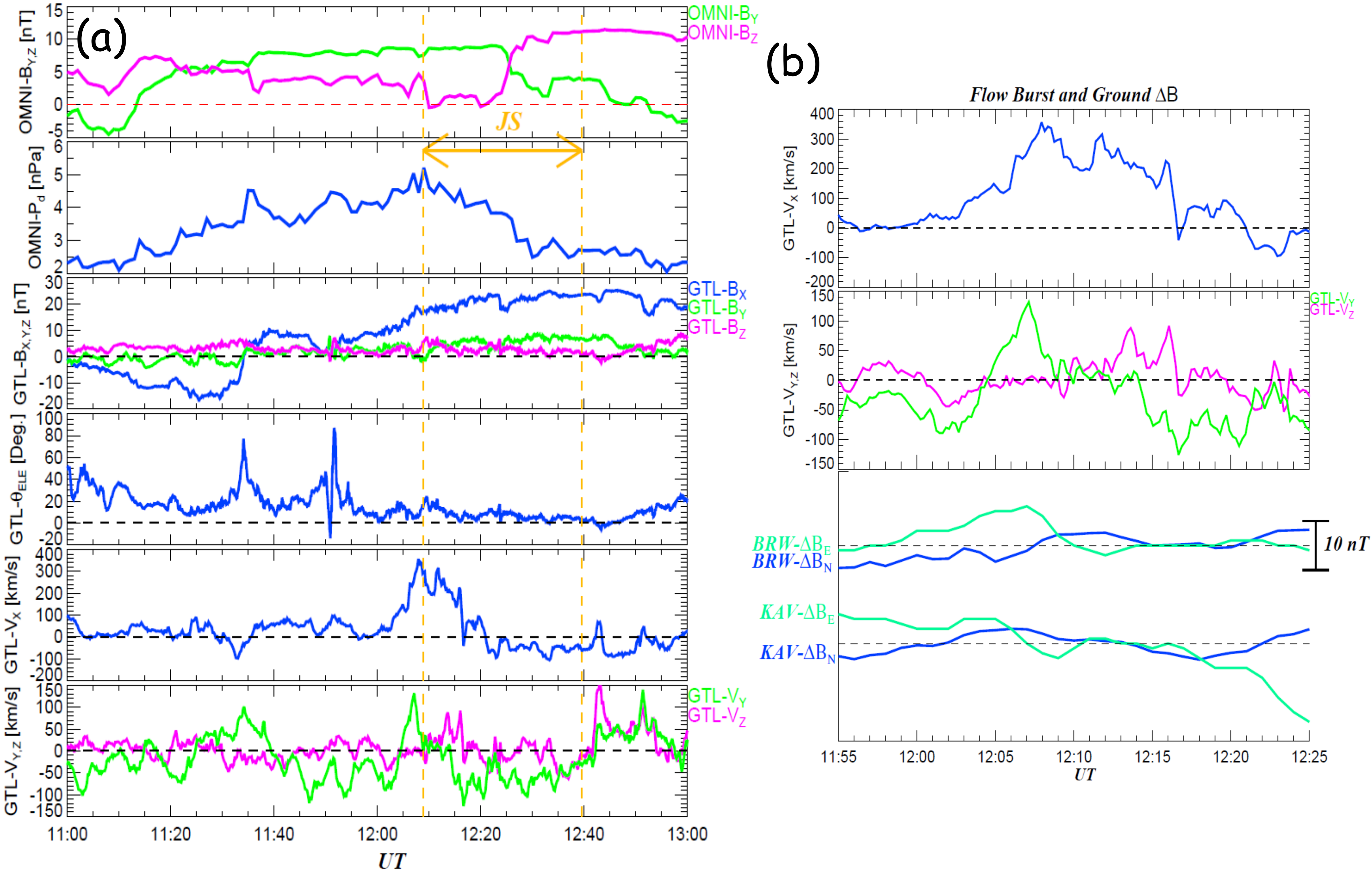

GTL Location during "J"-Shaped TPA in GSM: (-29.41, -9.71, 2.28)

Figure S2. The plots of in-situ dawnside magnetotail observation made by Geotail, corresponding solar wind conditions, and geomagnetic field variations at the observatories beneath and close to the proximity of the growth of the "J"-shape TPA seen on March 2nd, 2002 are displayed. Panel (a) shows a summary plot of the solar wind conditions obtained from the OMNI database and Geotail dawnside magnetotail observations for 2 hours between 11:00 UT and 13: 00 UT. From top to bottom panels show the IMF-B_y and -B_z components in GSM coordinate system, solar wind dynamic pressure calculated by $m_p N_p V_{sw}^2$, where m_p, N_p, and V_{sw} indicate the mass of proton, number density and solar wind velocity, the three components of the dawnside magnetotail magnetic field in GSM, associated magnetic field elevation angle obtained by $B_z/\mathrm{sqrt}(B_x^2 + B_y^2)$, and GSM-X, -Y, and -Z plasma velocity components in the dawnside magnetotail, respectively. The "J"-shaped TPA interval is bracketed by two gold broken lines with a label "JS" and two-heads arrow. The Geotail location during the "J"-shaped TPA interval is shown in the bottom of the panels. Panel (b) shows the zoomed-up three plasma flow velocity components in GSM, including the positive V_x enhancements which are suggestive of earthward plasma flow burst, and corresponding ground magnetic field variations observed at two representative magnetic observatories close to the "J"-shaped TPA. The ground magnetic field fluctuations are calculated by a subtraction of the magnetic field average during the presented interval from observed magnetic field data.

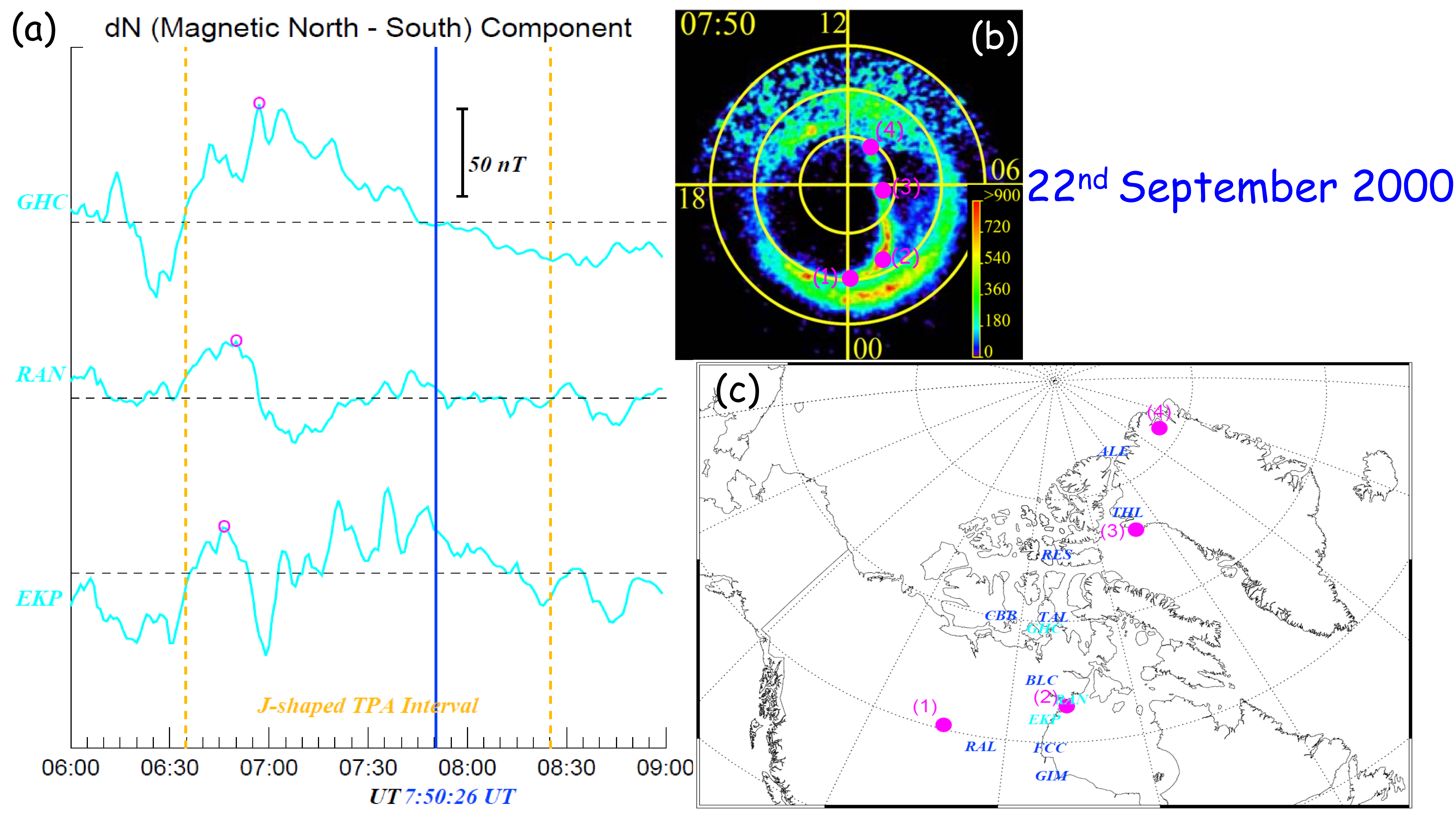
(a)
dN (Magnetic North - South) Component
GHC
RAN
EKP
50 nT
J-shaped TPA Interval
06:00
06:30
07:00
07:30
08:00
08:30
09:00
UT 7:50:26 UT
(b)
07:50
12
06
18
00
(1)
(2)
(3)
(4)
>900
720
540
360
180
0
22nd September 2000
(c)
ALE
THL
RES
CBB
TAL
GHC
BLC
RAN
EKP
RAL
FCC
GIM

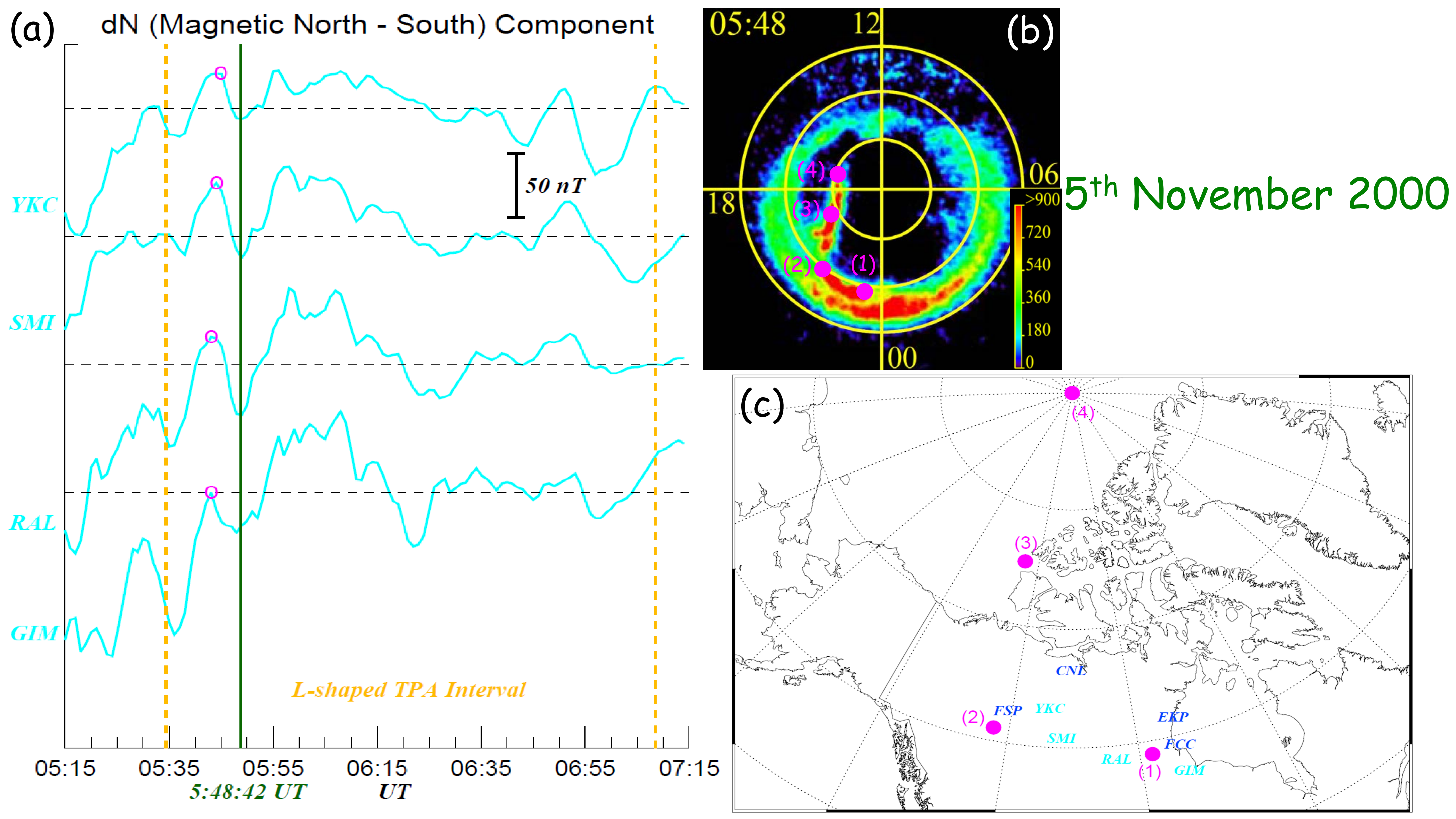

(a)
dN (Magnetic North - South) Component
YKC
SMI
RAL
GIM
50 nT
L-shaped TPA Interval
05:15
05:35
05:55
06:15
06:35
06:55
07:15
5:48:42 UT
UT
(b)
05:48
12
06
18
00
(1)
(2)
(3)
(4)
>900
720
540
360
180
0
5th November 2000
(c)
(1)
(2)
(3)
(4)
CNL
FSP
YKC
SMI
EKP
FCC
RAL
GIM

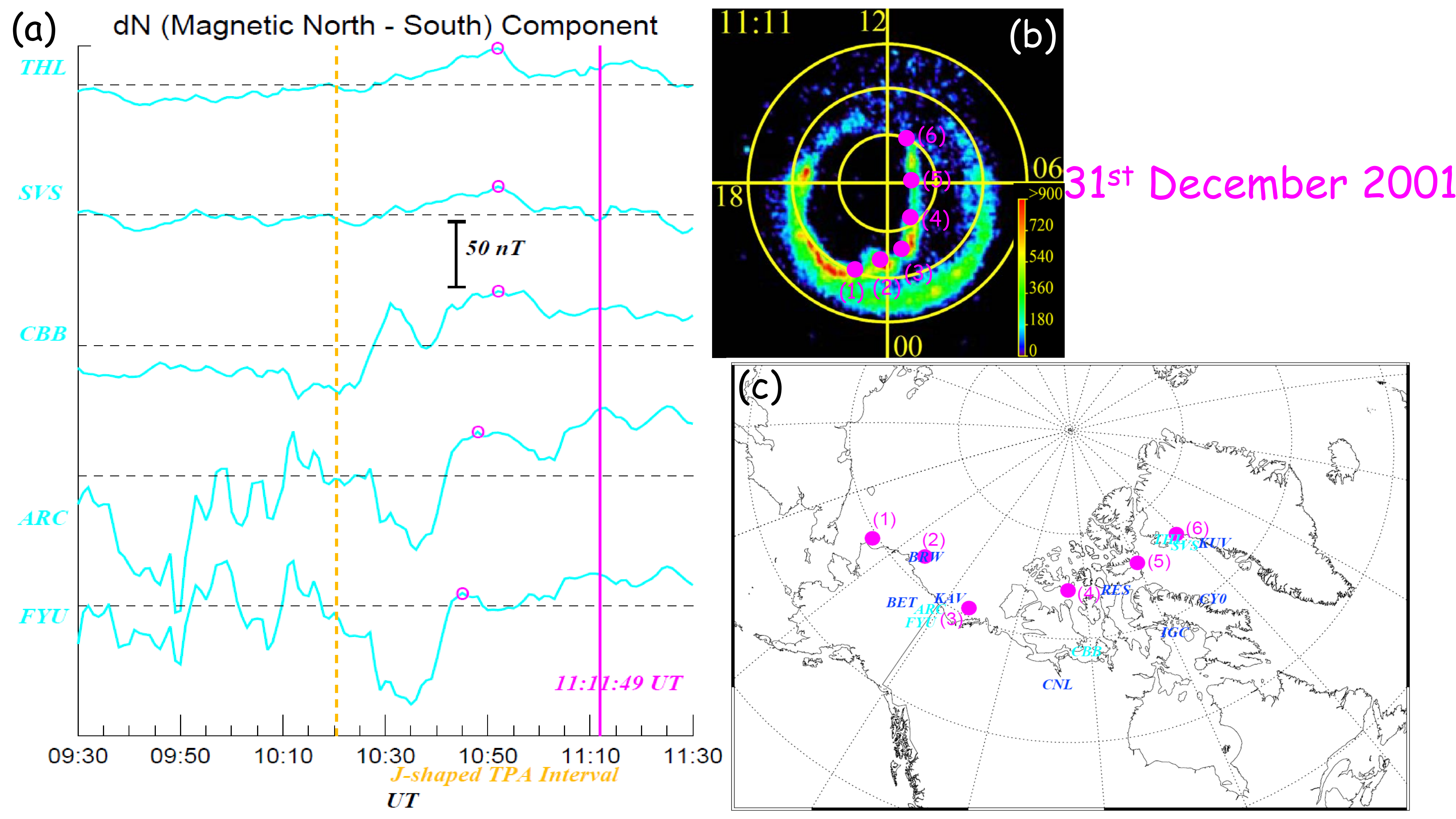
(a)
dN (Magnetic North - South) Component
THL
SVS
CBB
ARC
FYU
50 nT
11:11:49 UT
09:30
09:50
10:10
10:30
10:50
11:10
11:30
J-shaped TPA Interval
UT
(b)
11:11
12
06
18
00
(1)
(2)
(3)
(4)
(5)
(6)
>900
720
540
360
180
0
31st December 2001
(c)
(1)
(2)
(3)
(4)
(5)
(6)
BRW
BET
KAV
ARC
FYU
RES
CY0
IGC
CBB
CNL
KUV

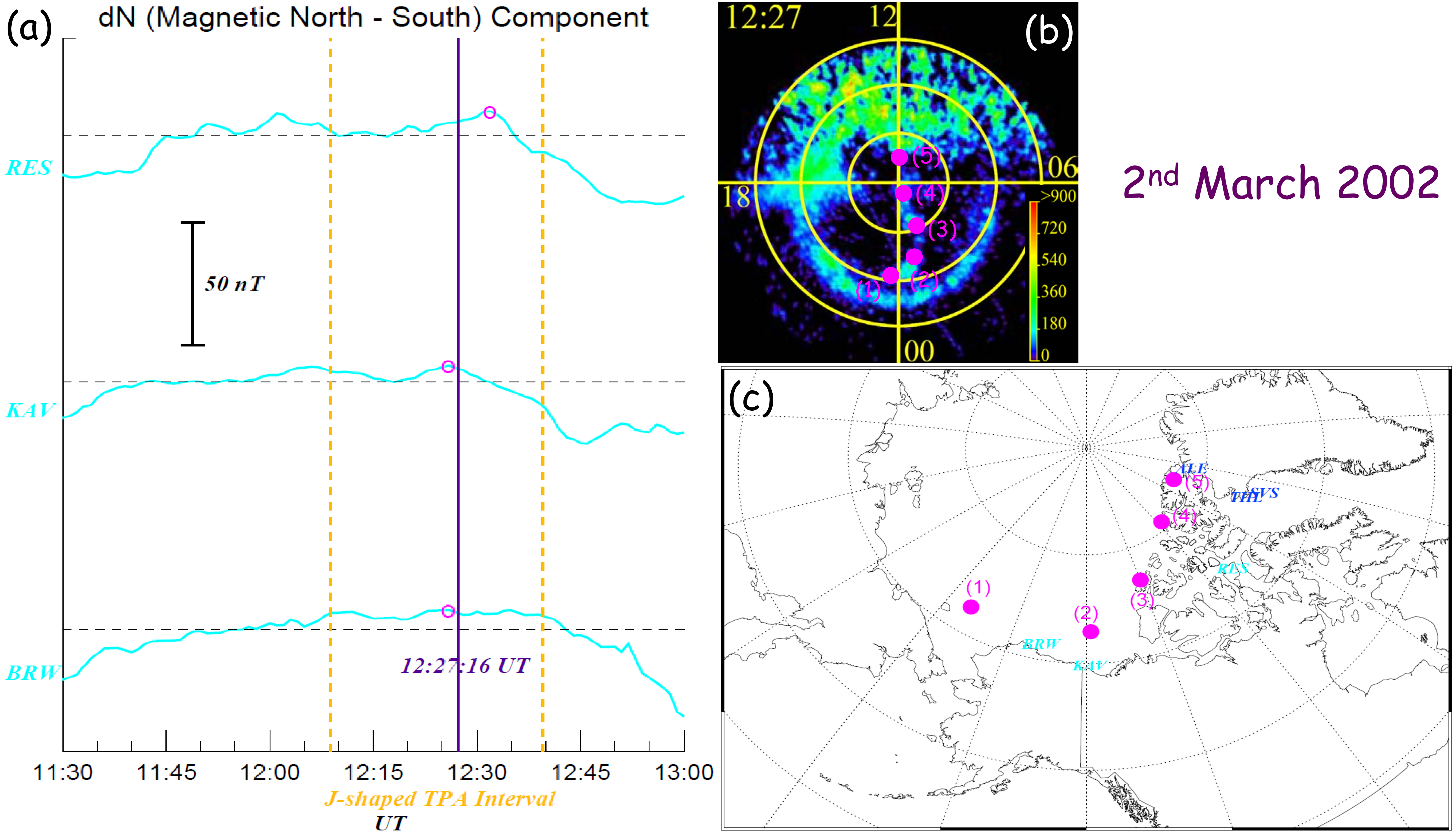
(a)
dN (Magnetic North - South) Component
RES
KAV
BRW
50 nT
12:27:16 UT
11:30
11:45
12:00
12:15
12:30
12:45
13:00
J-shaped TPA Interval
UT
(b)
12:27
12
06
18
00
>900
720
540
360
180
0
(1)
(2)
(3)
(4)
(5)
(c)
ALE
SVS
THL
RES
BRW
KAV
2nd March 2002

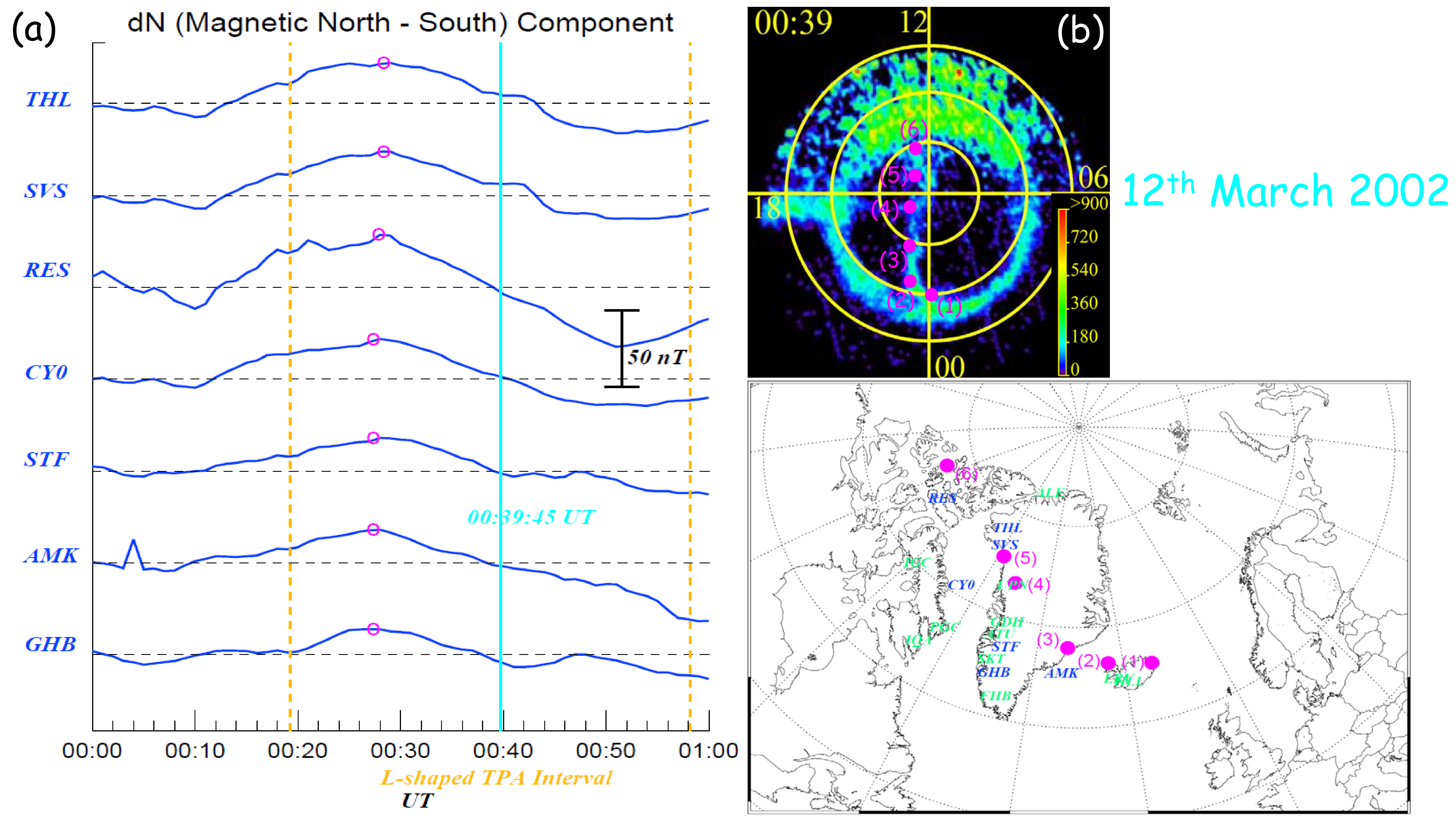

(a)
dN (Magnetic North - South) Component
THL
SVS
RES
CY0
STF
AMK
GHB
50 nT
00:39:45 UT
00:00
00:10
00:20
00:30
00:40
00:50
01:00
L-shaped TPA Interval
UT
(b)
00:39
12
06
18
00
>900
720
540
360
180
0
(1)
(2)
(3)
(4)
(5)
(6)
12th March 2002
RES
ALE
THL
SVS
CY0
STF
GHB
AMK
FHB
SKT
GDH
POC
IQA

Figure S3. The plots of in-situ geomagnetic magnetic field variations beneath and close proximity to the regions of growth of the 5 nightside distorted TPAs are displayed. Panels (a) to (c) show the magnetic field observational results at several ground magnetic observatories corresponding to the locations beneath or close proximity to the growth regions of the nightside distorted TPAs. Several magenta points labelled with numbers in the IMAGE FUV-WIC plots (panel b) correspond to similarly labelled locations in geographical map (panel c). Panel (a) shows the plots of fluctuations in the local magnetic north-south magnetic field component (ΔB_N) at these observatories highlighted by cyan or blue. The fluctuation component at each station is plotted upon their averages as indicated by horizontal grey broken lines, and its peak during the "J"- and "L"-shaped TPA intervals (bracketed by two gold broken lines) is marked by magenta open circle. The plots are sorted in decreasing order of latitude. The magnetic field fluctuation component at the time of panel (b) is indicated by a horizontal solid line in the panel. The color code of the IMAGE FUV-WIC data is assigned according to ADU.

Table S1. Fundamental information on the 9 nightside distorted TPA events used in this study, and values of key parameters on the associated magnetospheric conditions are summarized.

	Event Date	TPA Interval (UT)	Duration Interval (minutes)	Type of Nightside Distorted TPA	IMF-B_z Direction	IMF-B_y Direction	Average *AL*/*AU* [nT]	K_p	Ground-Based Observation	IMAGE N/S Hemisphere
I	2000/9/22	6:34:53 – 8:25:08	110	J	Northward	Dawnward	-40/80	2-	Yes (Data Used)	NH
II	2000/11/5	5:34:24 – 7:08:24	94	L	Northward	Duskward	-100/50	3+	Yes (Data Used)	NH
III	2000/12/27	23:31:42 – 00:33:05	63	J	Northward to Southward	Dawnward to Duskward	-18/23	2-	Yes (No Used) †1	NH
IV	2001/12/31	10:20:34 – 14:40:46	260	J	Northward	Dawnward	-25/90	1+	Yes (Data Used)	NH
V	2002/3/02	12:08:49 – 12:39:34	31	J	Northward	Duskward	-29/25	1+	Yes (Data Used)	NH
VI	2002/3/12	00:19:16 – 00:58:12	39	L	Northward	Duskward	-31/44	2+	Yes (Data Used)	NH
VII	2003/10/28	13:20:18 – 14:17:55	58	L	Northward	Duskward	-295/40	3-	Yes (No Used)†2	NH
VIII	2004/6/5	9:42:37 – 10:15:44	33	L	Northward to Southward	Dawnward	-25/90	2+	No	SH
IX	2005/6/1	11:28:38 – 12:14:28	46	J	Northward	Dawnward to Duskward	-58/25	2-	No	SH

†1 Neither peaks nor variations in the geomagnetic field during the interval of the nightside distorted TPA were found.

†2 The clear peaks cannot be identified because of highly magnetic fluctuations during the interval of the nightside TPA.

Table S2. The station code, geographical longitude (GEOLon), latitude (GEOLat), geomagnetic longitude (MLon), latitude (MLat), and station name are listed with the order from high- to low-latitudes in geographic coordinates (GEOLat). The magnetic field data obtained from these ground stations are used to draw the electric current vectors as shown in Figure 3.

Station Code	GEOLon [deg.]	GEOLat [deg.]	MLon [deg.]	MLat [deg.]	Station Name
UPN	303.85	72.78	41.35	79.45	Upernavik
CY0	291.4	70.5	18.56	79.18	Clyde River
SCO	338.03	70.48	72.73	71.56	Ittoqqortoormiit
IGC	278.2	69.3	-7.6	79.08	Igloolik
GDH	306.47	69.25	40.09	75.73	Godhavn
ATU	306.43	67.93	38.76	74.47	Attu
STF	309.28	67.02	41.46	73.06	Kangerlussuaq
PGC	294.2	66.1	20.27	74.74	Pangnirtung
AMK	322.37	65.6	54.24	69.15	Tasiilaq
SKT	307.1	65.42	37.63	71.89	Maniitsoq
LRV	338.3	64.18	67.25	64.85	Leirvogur
GHB	308.27	64.17	38.22	70.43	Nuuk
HLL	339.44	63.77	67.9	64.23	Hella
IQA	291.48	63.75	15	72.9	Iqaluit
FHB	310.32	62	39.35	67.82	Paamiut